Faculté des Sciences de la Nature et de la Vie
Département de Microbiologie et de Biochimie

Cours

Méthodologie de Recherche

La présentation affichée (Poster)

Cours élaboré par Dr BOUDIAF K,, Présenté pour les étudiants L1
Par Pr AISSAT K.

Qu'est-ce qu'un poster scientifique?

- Le poster est un moyen de **présentation** d'un travail scientifique
- Il s'agit d'une méthode populaire et efficace de communication lors des **rencontres scientifiques** (congrès)
- En fonction de la conférence, le nombre de posters peut varier d'une douzaine à plusieurs centaines

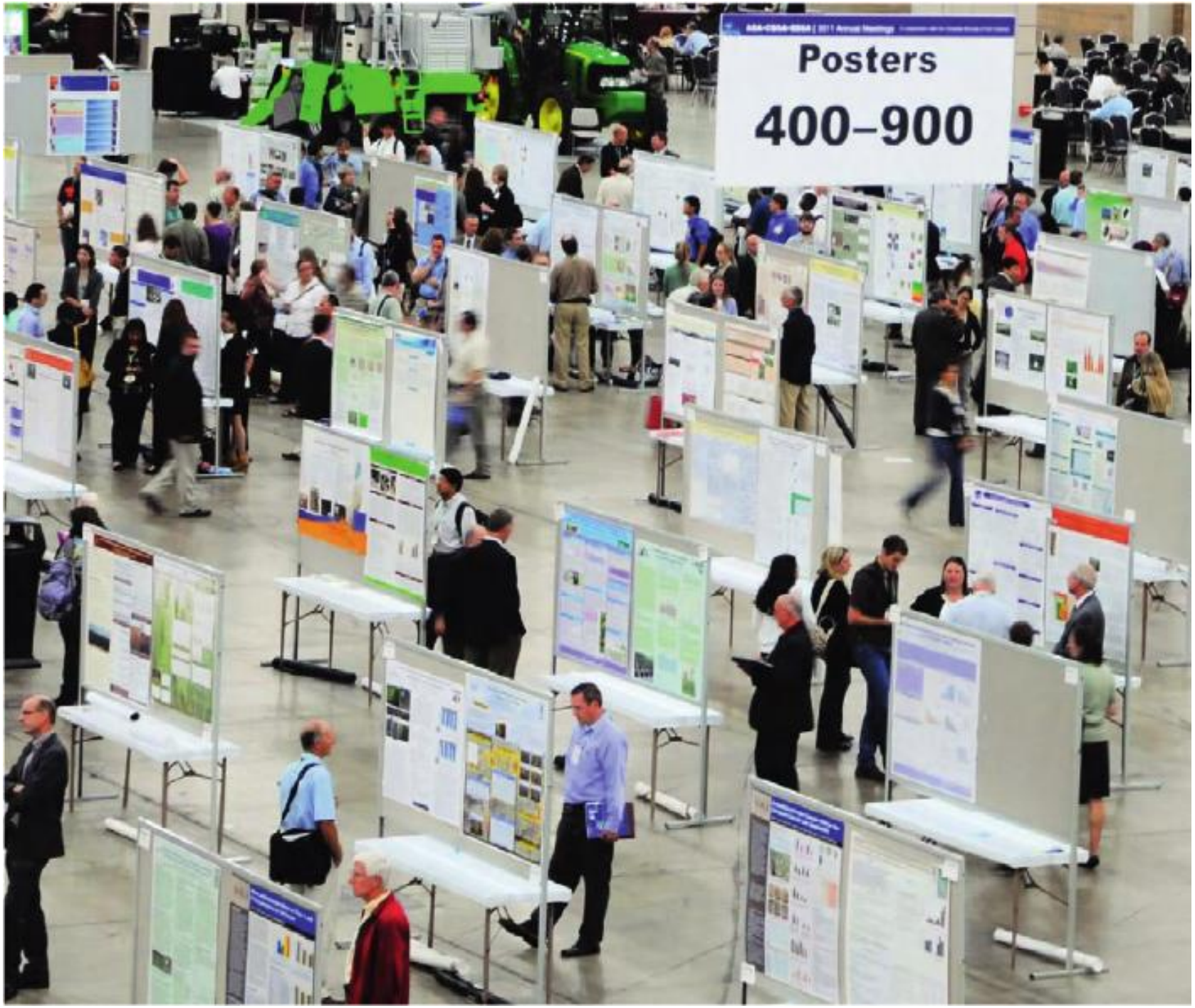
Posters
400–900

Objectifs *du poster scientifique*

Communiquer sur son travail (congrès, rencontres professionnelles):

- **Susciter la curiosité**
- **Capter l'attention**
- **Provoquer les échanges**

Le poster doit être Efficace

- **Attractif**

  pour capturer l'attention

- **Structuré**

  pour favoriser la lecture

- **Concis**

  pour axer la communication sur le message

Le poster doit être Attractif

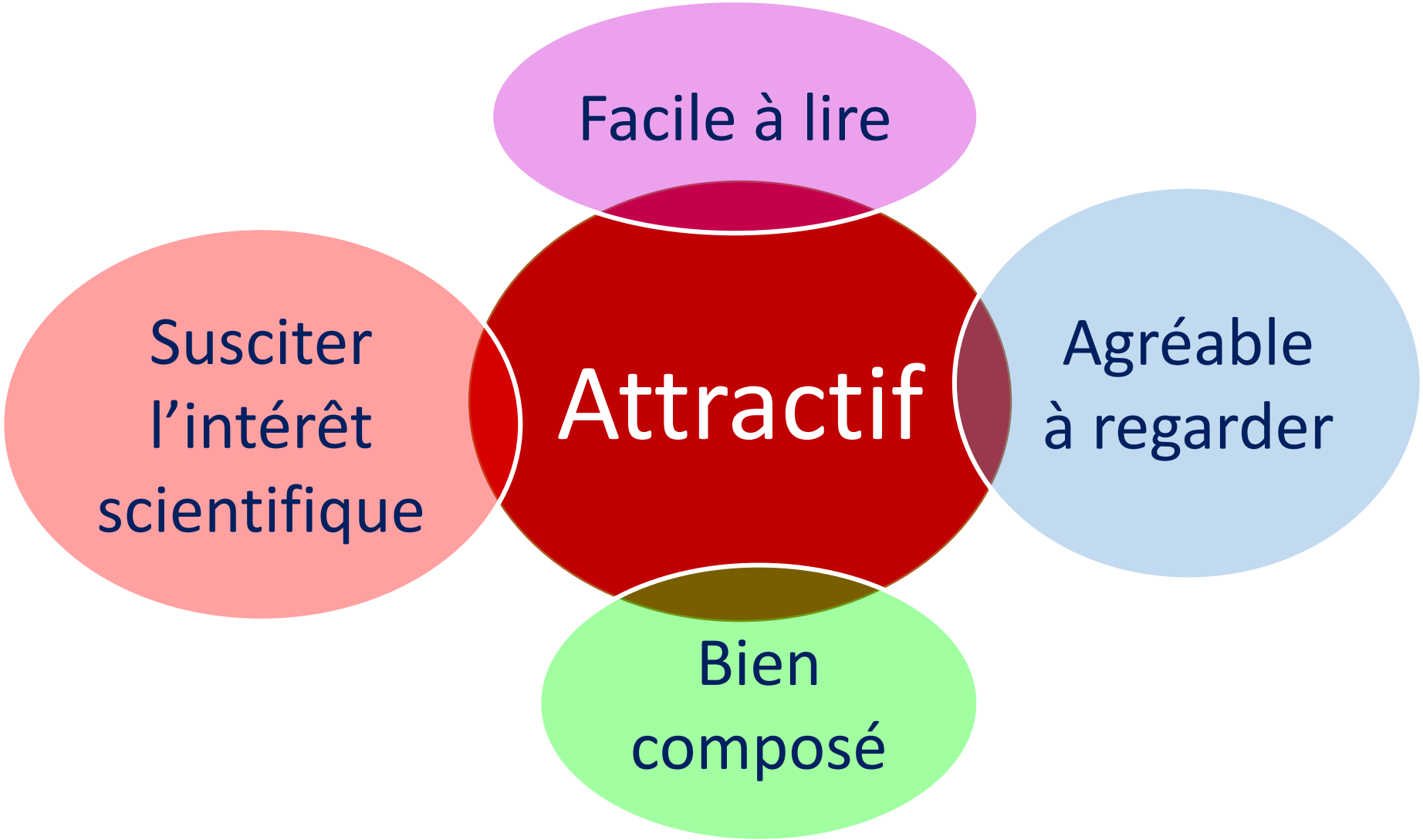

Contre exemple d'attractivité

Sans commentaires !

Sur ce poster,
personne ne s'arrêtera …

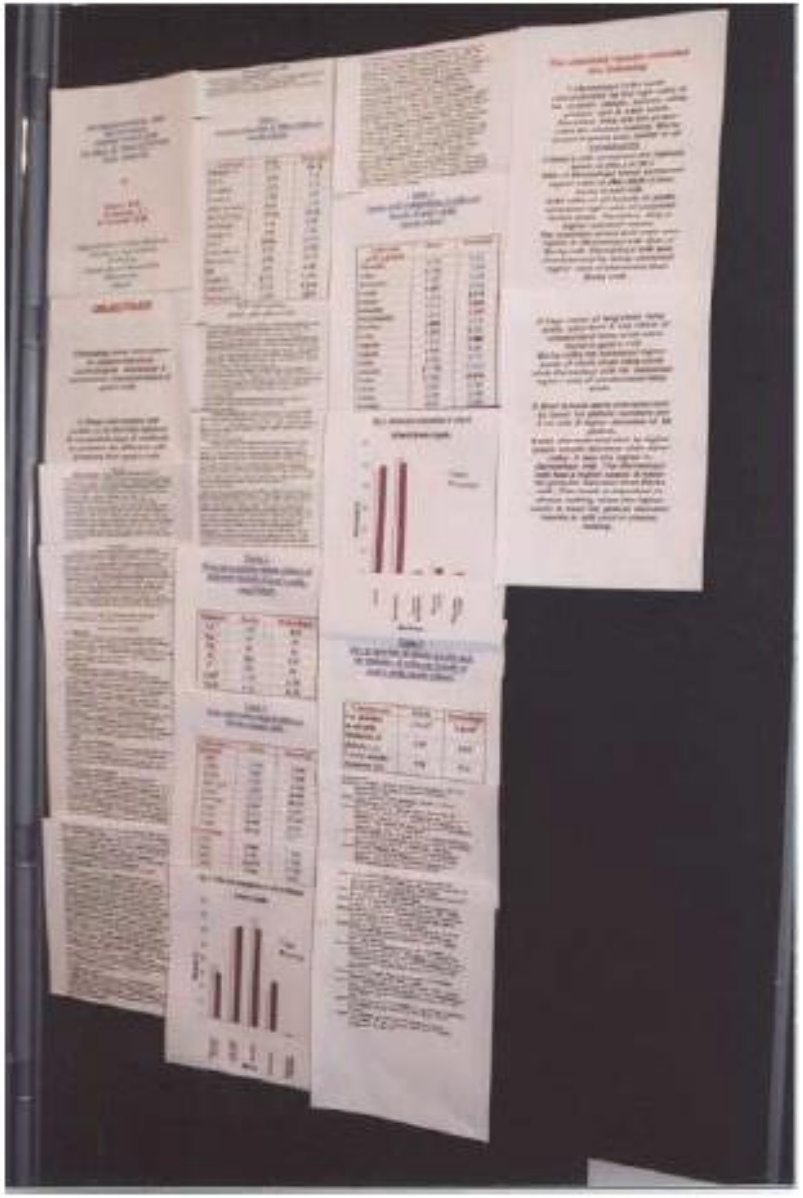

Structure et réalisation du poster scientifique

Structure du poster scientifique

Pour concevoir le poster, se souvenir qu'il doit être :

- Un **résumé** des recherches que vous avez faites
- Une **image** qui donne envie de s'approcher
- Un **spectacle** pour le lecteur qui s'y arrête 5 minutes maximum
- Un **message** qui cherche à convaincre le lecteur

Structure du poster scientifique

- Un poster scientifique doit comprendre toutes les parties d'un rapport de recherche habituel (**IMRAD**):
  - Une **I**ntroduction théorique
  - La **M**éthodologie
  - Les **R**ésultats
  - La **D**iscussion

Structure du poster scientifique

Section	
Titre	
Nom des auteurs	
Adresse des auteurs (+/- email)	
Introduction	Clairs et brefs
Objectif	Pas de revue de littérature
Méthodes	Si possible, illustré
Résultats	De préférence illustrés (sans texte)
Discussion/Conclusion	Conclusion bien visible
Références	
Remerciements	

→ **Texte réduit au minimum**

Table 6.2 Posters checklist

Section
Title
Names of authors or contributors
Address of authors or contributors
Keywords
Brief introduction
Methods used
Results
Discussion/Conclusions
References
Acknowledgements

Structure du poster scientifique

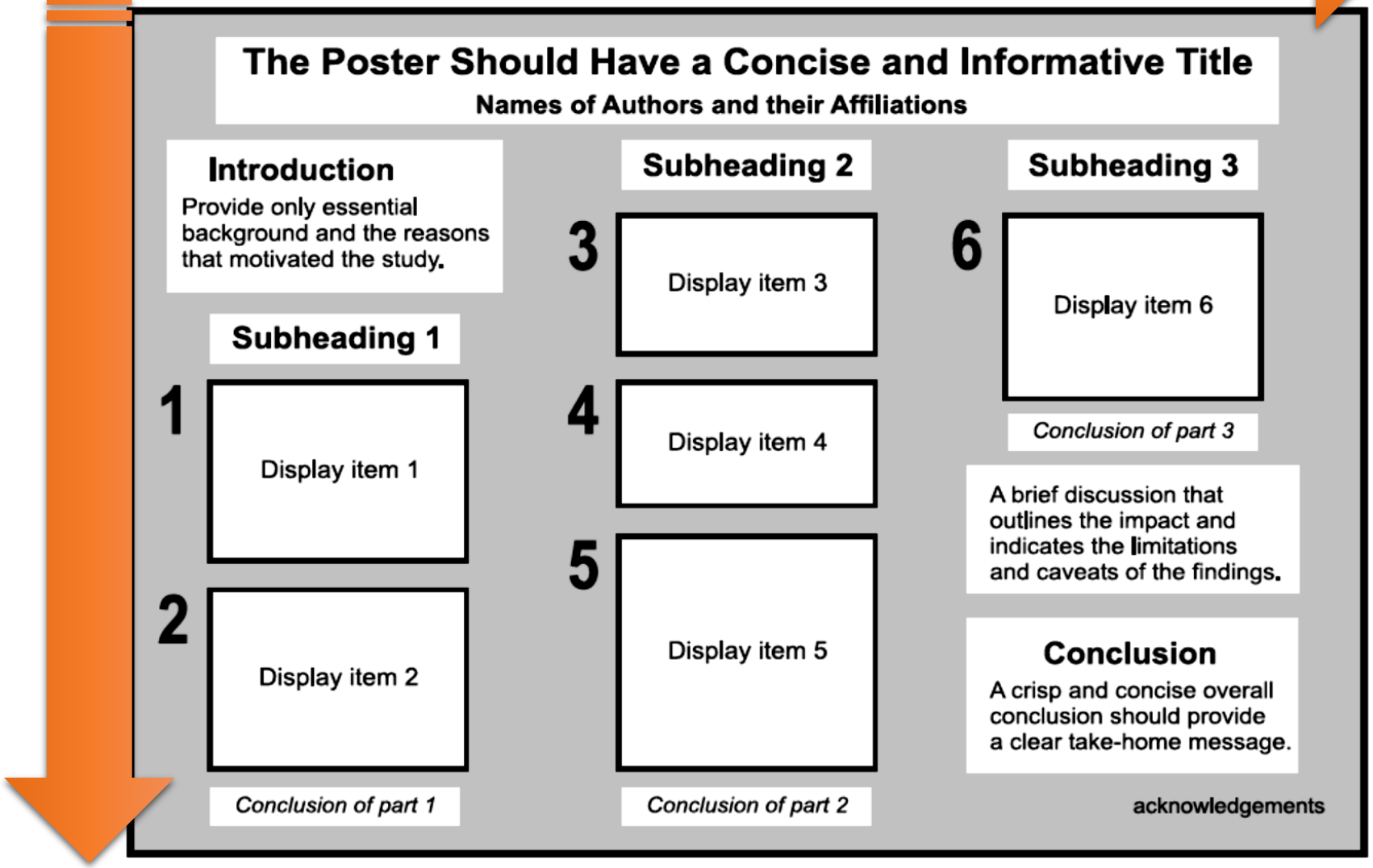

Structure du poster scientifique

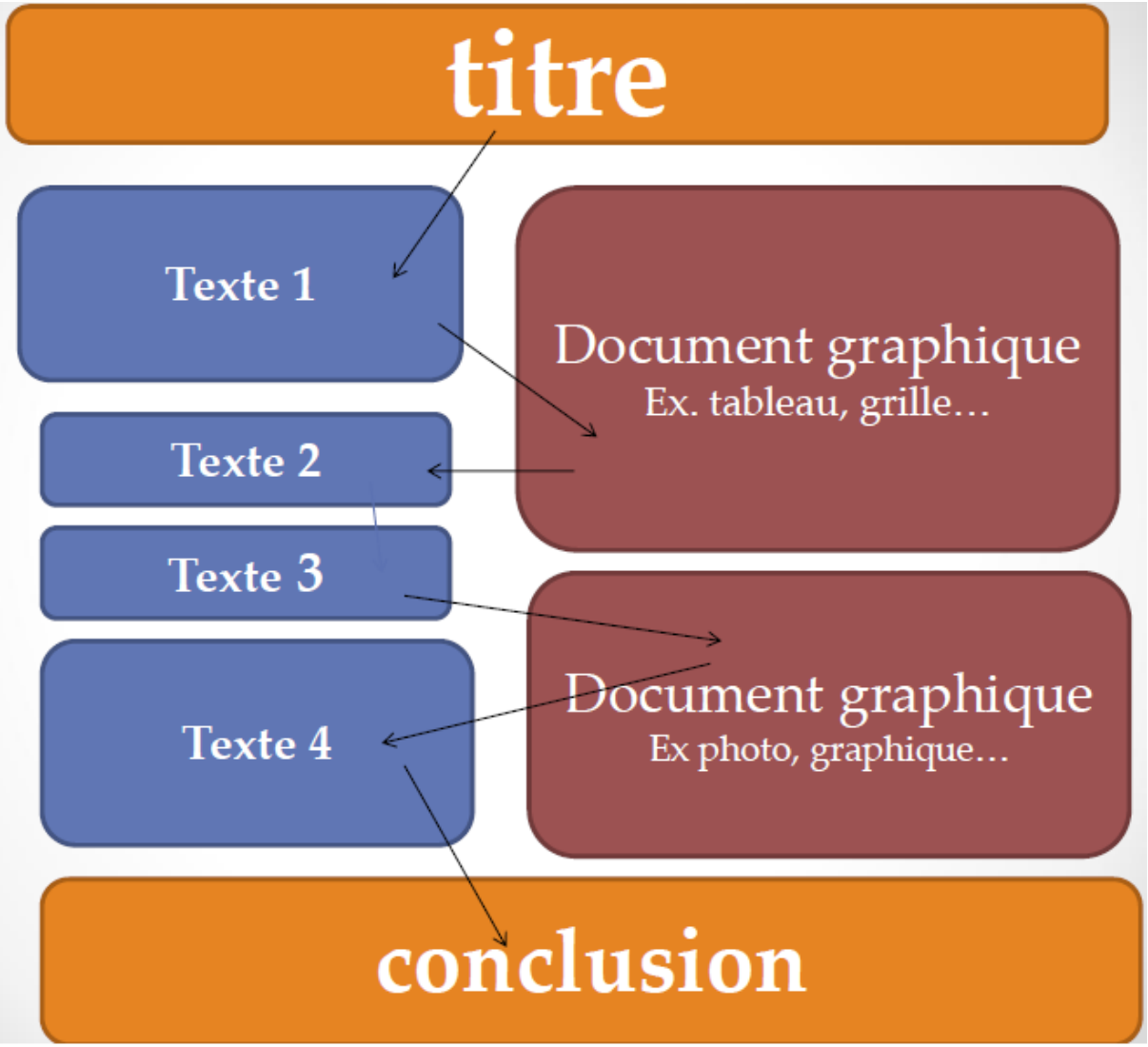

Réalisation du poster scientifique

- En 3 étapes:

1) **Le scénario**

2) **Le story-board (découpage du scénario)**

3) **La réalisation**

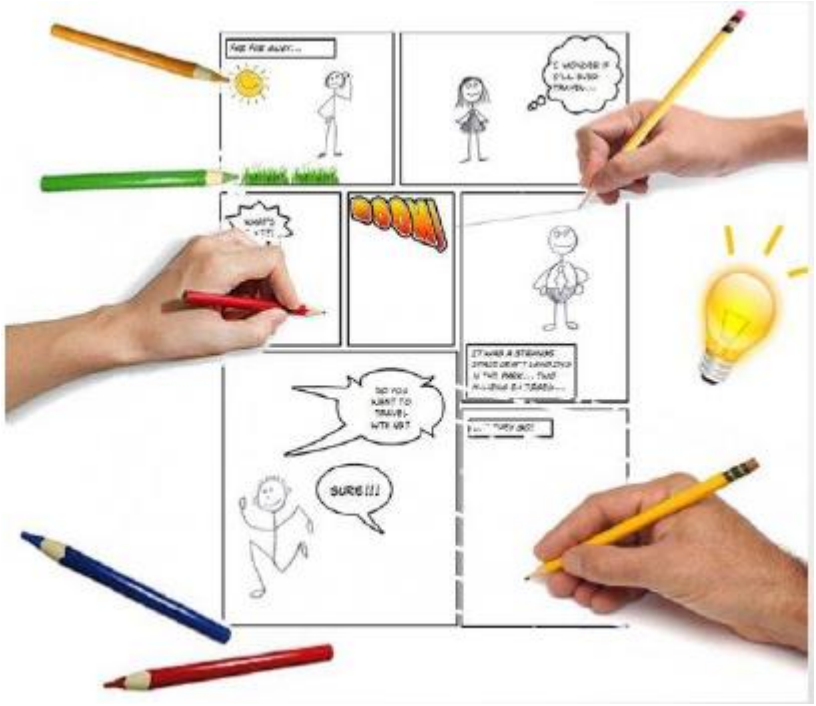

Réalisation du poster scientifique

Proportions:

- **30%** de texte
- **40%** d'illustrations
- **30%** de vide

Eviter:

- La belle affiche avec trop peu d'information
- L'affiche bien pleine mais invisible

Réalisation du poster scientifique

Prêter attention à :

- **Choix des couleurs (texte/fond)**

(meilleur : texte noir sur fond blanc)

- **Police et taille du texte**

(Sans sérif, non majuscule, non italique)

Content	Reading distance (m)	Size (point)	Style of type
Title	3–4	72–96	**Bold**
Authors	3–4	54–72	**Bold**
Main headings	2+	48–54	**Bold**
Sequence numbers	2+	36	Regular
Main text	1+	24–28	Regular, single spacing
Detail text	1+	18–24	Regular

Exemples de Mauvais poster

NC STATE UNIVERSITY

Southern Flounder Exhibit Temperature-Dependent Sex Determination

J. Adam Luckenbach*, John Godwin and Russell Borski

Department of Zoology, Box 7617, North Carolina State University, Raleigh, NC 27695

Introduction

Southern flounder (*Paralichthys lethostigma)* support valuable fisheries and show great promise for aquaculture. Female flounder are known to grow faster and reach larger adult sizes than males. Therefore, information on sex determination that might increase the ratio of female flounder is important for aquaculture.

Objective

This study was conducted to determine whether southern flounder exhibit temperature-dependent sex determination (TSD), and if growth is affected by rearing temperature.

Methods

- Southern flounder broodstock were strip spawned to collect eggs and sperm for *in vitro* fertilization.
- Hatched larvae were weaned from a natural diet (rotifers/*Artemia*) to high protein pelleted feed and fed until satiation at least twice daily.
- Upon reaching a mean total length of 40 mm, the juvenile flounder were stocked at equal densities into one of three temperatures 18, 23, or 28°C for 245 days.
- Gonads were preserved and later sectioned at 2-6 microns.
- Sex-distinguishing markers were used to distinguish males (spermatogenesis) from females (oogenesis).

Histological Analysis

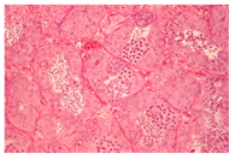

Male Differentiation

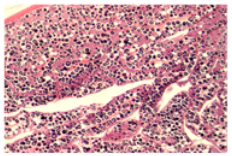

Female Differentiation

Temperature Affects Sex Determination

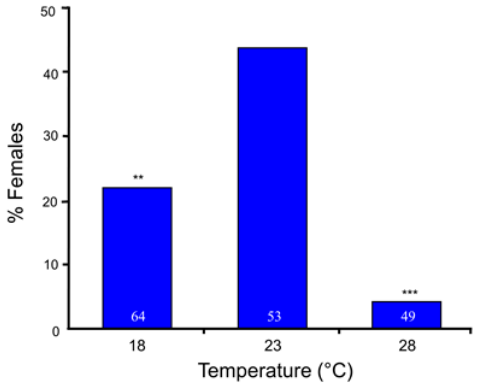

(**P < 0.01 and ***P < 0.001 represent significant deviations from a 1:1 male:female sex ratio)

Rearing Temperature Affects Growth

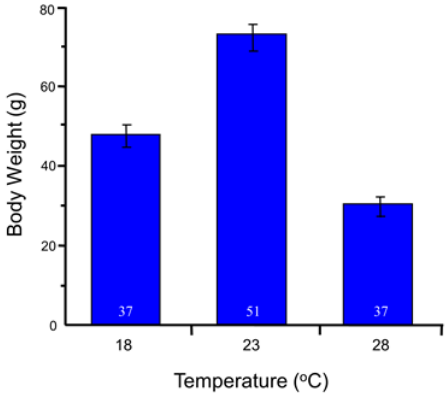

Growth Does Not Differ by Sex

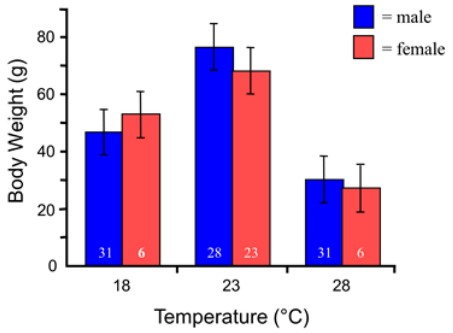

Results

- Sex was discernible in most fish greater than 120 mm long.
- High (28ºC) temperature produced 4% females.
- Low (18ºC) temperature produced 22% females.
- Mid-range (23ºC) temperature produced 44% females.
- Fish raised at high or low temperatures showed reduced growth compared to those at the mid-range temperature.
- Up to 245 days, no differences in growth existed between sexes.

Conclusions

- These findings indicate that sex determination in southern flounder is temperature-sensitive and temperature has a profound effect on growth.
- A mid-range rearing temperature (23°C) appears to maximize the number of females and promote better growth in young southern flounder.
- Although adult females are known to grow larger than males, no difference in growth between sexes occurred in age-0 (< 1 year) southern flounder.

Acknowledgements

The authors acknowledge the Salstonstall-Kennedy Program of the National Marine Fisheries Service and the University of North Carolina Sea Grant College Program for funding this research. Special thanks to Lea Ware and Beth Shimps for help with the work.

On using phylogenetically independent contrasts to identify most parsimonious cladograms

Amanda G. Henry

Center for Advanced Study of Hominid Paleobiology
Department of Anthropology
The George Washington University

Introduction

When reconstructing relationships among fossil hominins, scientists often rely on craniodental traits, since these are usually the best preserved. While several researchers support the use of masticatory traits (Collard and Wood, 2001; Lycett and Collard, 2006), others have raised concerns about homoplasy in the craniodental system (Andrews and Martin, 1991; Begun, 1994; Lieberman et al., 1996; Skelton and McHenry, 1992). Because of these debates, those researchers who create cladograms often choose to exclude, or at least to give less weight to characters derived from the masticatory system when attempting to reconstruct the relationships among living primates as well as fossil hominins.

In attempt to find another way around this problem of homoplasy, I propose to look for a different method to use masticatory traits to discern the cladistic relationships among taxa. While the relationship between body size and mandible size has been considered (Bouvier, 1986; Plavcan, 2003; Wood and Aiello, 1998), scaling of tooth size to mandible size has yet to be used as a phylogenetic trait. Lucas (2004) has shown that there are several scaling relationships between body size, mandible size, and tooth size. In brief, smaller animals have smaller mandibles, and their anterior teeth match this mandible size. These features control the size of the particle taken into the mouth. However, smaller food particles tend to fracture at larger stress than larger food particles, so a smaller animal needs relatively larger posterior teeth than a larger animal. This creates a negative allometry between mandible size and posterior teeth size - as mandible size increases, so does molar size, but at a slower rate. Different lineages, however, may have slightly different scaling relationships between teeth size and jaw size, and these different scaling patterns may be used to test phylogenetic relationships.

Scaling relationships between mandible size and molar size

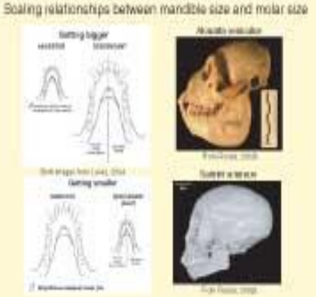

PIC and 'reverse' PIC

Phylogenetically Independent Contrasts (PIC) is designed to test for correlated evolutionary change between two variables (Nunn and Barton, 2001). It works by calculating the distance between sister taxa on a tree, and normalizing this distance based on branch length. These distances, or contrasts, are then plotted, and the correlation coefficient for the contrasts is calculated. Because confounding variables due to shared descent are removed in this analysis, the scaling relationships found among contrasts are more dependent on the traits in question, and less likely to show a relationship where there is none. Points that represent a major shift in the relationship between the two variables, like grade shifts, appear as outliers on the plot.

PIC is generally used to test whether certain characters are correlated, with the assumption that the starting tree is the correct one. I am attempting to use this method **in the opposite order**. I am testing whether, by using traits for which we are confident there is correlated evolutionary change, we can identify the most parsimonious cladogram based on the correlation coefficient calculated in PIC. Because we believe there is tight correlated evolutionary change and a strong allometric relationship between mandible area and molar area that is likely conserved within a lineage, the tree showing the true phylogenetic relationship should show the highest correlation between the contrasts of these variables. Trees not showing the true phylogenetic relationship should have lower correlation.

The process of Phylogenetically Independent Contrasts

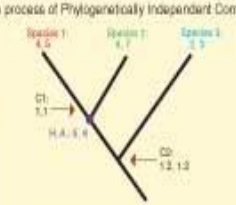

Contrast 1 = (X2-X1)/Branch Length
and (Y2-Y1)/Branch Length
= 1, 1

Hypothetical ancestor 1 = (X1+X2)/2
and (Y1+Y2)/2
= 5, 6

Contrast 2 = (X-X3)/B.L.
and (Y-Y3)/B.L.
= 1.2, 1.2

Etc...

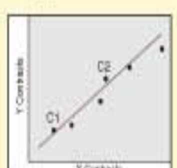

Four proposed cladograms for NWM:

The plot of contrasts for each cladogram:

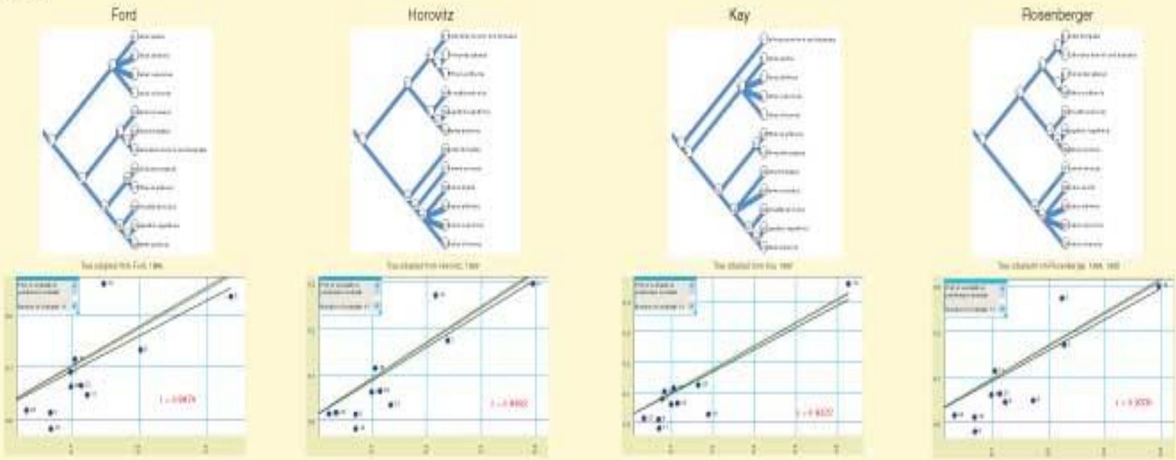

Using 'reverse' PIC on primate data

To test 'reverse' PIC, I used a dataset of New World monkey M2 and mandible at M2 areas[1], and averaged them for each species. I entered these data into Mesquite (Maddison and Maddison, 2004), along with several different cladograms for these species taken from the literature (Kay, 1990; Ford 1986, Horovitz, 1999; Rosenberger, 1984, 1992). One of these cladograms, Horovitz, was based on DNA, so therefore I used the Horovitz cladogram as the 'true' tree. If PIC works in reverse to identify true trees, then the Horovitz tree should have the highest correlation coefficient and the others should have noticeably lower ones.

The plots of the contrasts calculated for each tree through PIC are shown above. The tree based on masticatory traits, Kay, has the highest correlation coefficient. The Horovitz tree has the second highest correlation coefficient. However, the Kay tree is strongly weighted by the contrast labeled #14. Because this point is an outlier, I recalculated the correlation coefficient without this contrast. The new correlation coefficient dropped to 0.368, making it insignificant even at $p = 0.1$. In order to test whether simply removing the point to the furthest right causes the correlation coefficient of any tree to become insignificant, this process was repeated for the other trees. In these three cases, the correlation coefficient values were still significant at $p < 0.025$, making it likely that only in the Kay tree does this top right point significantly effect the correlation. Therefore, the Kay tree does not in fact have the best correlation. Once the outlier has been discounted, the Horovitz tree has the highest correlation coefficient, showing that 'reverse' PIC does identify the most parsimonious cladogram.

Finally, in an effort to test how well one can distinguish which tree has the best correlation, the 95% confidence intervals for each correlation coefficient were calculated. Because the number of species and therefore the sample size was so small, all of the confidence intervals overlapped. Therefore, it is impossible to distinguish among these correlation coefficients, which prevents us from firmly identifying which tree is best.

[1] [illegible]

The NWM data entered into Mesquite

Species	Average log mandible area	Average log M2 area	Total specimens
Aotus trivirgatus	1.5695	1.0527	13
Callicebus moloch and torquatus	1.755	1.0601	13
Lagothrix lagotricha	2.1573	1.5118	10
Saimiri sciureus	1.3481	0.8203	13
Alouatta seniculus	2.2601	1.6462	40
Ateles paniscus	2.0577	1.4049	41
Cebus apella	2.0562	1.3276	110
Cebus olivaceus	1.8878	1.2623	59
Chiropotes satanas	2.0157	1.1578	40
Pithecia pithecia	1.9177	1.1342	42
Cebus albifrons	1.8941	1.2271	34
Cebus capucinus	1.8345	1.2631	23

Correlation coefficents (r) with and without top right contrast, significane value of r without top right contrast

Tree	R	R with one node removed	p value
Kay	0.9472	0.3668	not significant
Horovitz	0.9402	0.8522	<0.005
Rosenberger	0.9336	0.8251	>0.005
Ford	0.8970	0.6842	<0.025

Correlation coefficients and 95% confidence limits

Tree	R	95% Lower Limit	95% Upper Limit
Kay	0.9472	0.8380	0.9845
Horovitz	0.9402	0.8070	0.9824
Rosenberger	0.9336	0.7869	0.9804
Ford	0.8970	0.6830	0.9691

Conclusion

This analysis has shown that PIC is not limited to finding correlated traits, but can be used to test competing cladograms. 'Reverse' PIC can allow us to identify the most parsimonious cladogram based on the correlation coefficient, as with the Horovitz tree. It also enables us to see and therefore discount outliers, such as in the Kay tree. Unfortunately, PIC was not able to discriminate between trees in a statistically significant way given the data used here. There are several ways of improving the strength of 'reverse' PIC. One could employ different scaling relationships, like body size to mandible size, or group results from additional pairs of features. Other possibilities include taking into account not just the mean value but also the variance for each species, or increasing the number of species considered, so as to increase the sample size.

This analysis has shown it may be possible to use 'reverse' PIC on a scaling relationship involving craniodental traits. With some work to strengthen the method, we may be able use 'reverse' PIC as a technique to identify the most parsimonious cladogram for fossil hominins.

Bibliography and Acknowledgements

[illegible]

Isolating and Identifying Transcription Factors that Bind the Cd4 Promoter

Matthew C. Surdel and Sophia D. Sarafova

Davidson College Biology Department

I. Background and Observations

CD4 and CD8 cells are essential in immune system function. Both are classified as T-cells and derive from a common precursor, but only CD4 cells express the Cd4 gene. CD4 is a transmembrane glycoprotein that modulates the T-cell receptor signal and therefore the magnitude of the immune response. Having the correct amount and timing of Cd4 expression is essential for the proper development and function of the CD4 cells. Not surprisingly, Cd4 expression is a highly controlled process; regulatory elements found to date include a promoter (containing four binding sites – P1-P4), a silencer, a mature enhancer, and a thymocyte enhancer. In the promoter region, the proteins that bind to the P1, P2, and P4 regions have been identified, while P3 remains unknown as shown in Figure 1.

Previous research has shown a protein-DNA complex formation specific to the P3 sequence that does not form with the D06 sequence, which differs by only four base pairs from the P3 site but reduces promoter function by 80% (Figure 2 and data not shown). Furthermore it has been shown that this protein-DNA complex does not appear when using CD8 nuclear extract (Figure 2C), implying that CD8 cells may not contain this protein.

To further understand the control of Cd4 expression we wish to isolate and identify transcription factors that bind to the P3 site of the Cd4 gene promoter region. DNA affinity chromatography and SDS polyacrylamide gel electrophoresis (SDS-PAGE) were used to identify proteins that bound to the P3 DNA sequence, but not the D06 sequence. To ensure specificity of the transcription factor of interest we used the D06 mutant sequence as a specific competitor to P3 and vice versa. This protein would be the second transcription factor specific to CD4 cells identified to date.

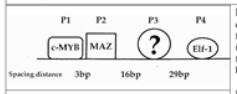

Figure 1 (Sarafova and Siu, 2000). A schematic diagram of the CD4 promoter and its binding factors. P1, P2, P3 and P4 are the functionally important binding sites. The distance between the four binding sites is shown in base pairs. The known binding factors for each site are indicated.

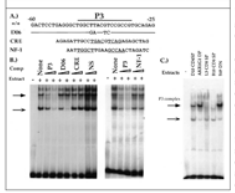

Figure 2 (Sarafova and Siu, 2000). Biochemical analysis of the P3 site. (**A**) The P3 sequence from the CD4 promoter is aligned with the consensus sequences for CREB-1 and NF-1. The two half sites of each consensus are underlined. Mutant D06, which causes a significant decrease of promoter activity (84%), is shown, aligned to the wild-type sequence. (**B**) EMSA of the P3 with CD4+CD8- D10 cell extract. Two complexes are indicated with a filled arrow and with a thin arrow. Non-radioactively labeled competitors are indicated above the lanes and are used in 50-200-fold molar excess. The sequence of the competitors is the same as in (A). (**C**) EMSA with extracts from five different cell lines and the P3 probe. The cell lines and their developmental stage are indicated above each lane. Complexes are labeled with arrows as in (B).

II. Goal

Isolate and identify the putative transcription factor that binds to the promoter region of the Cd4 locus at the P3 site.

III. Approach

To purify the protein of interest, we used the known region from the Cd4 locus (P3) and a mutant form of that region (D06) that does not bind the protein we are looking for.

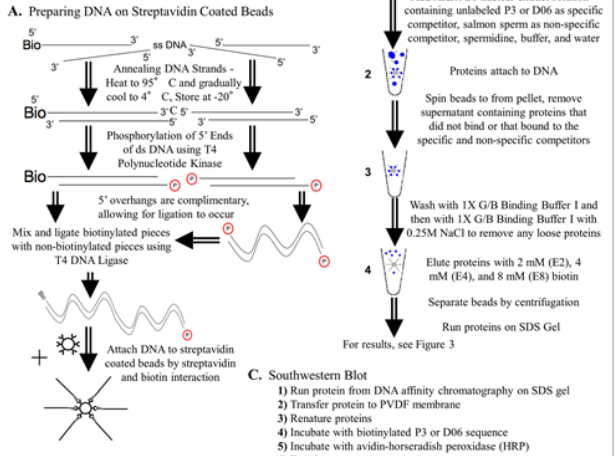

IV. Results

After successful completion of DNA affinity chromatography and SDS-PAGE, one distinct band was seen (Figure 3). This band represents proteins that were pulled down using DNA affinity chromatography with the P3 sequence that were absent when D06 was used indicating specificity for the P3 sequence (shown in Figure 3).

This band was analyzed by liquid chromatography tandem mass spectrometry (LC-MS/MS) at Duke Proteomics. The data was viewed in Scaffold (Figure 4). A transcription factor, upstream binding factor (UBF), was present in the P3 E2 and E4 bands and was of the correct molecular weight. UBF however does not meet the requirements to be the transcription factor of interest - it is slightly smaller, does not specifically bind DNA, and recruits RNA polymerase I and not RNA polymerase II (Figure 5).

To determine if our DNA affinity chromatography did in fact purify a protein specific for the P3 sequence, a southwestern blot was performed. Results show a band present in nuclear extract and purified protein using the P3 sequence and DNA affinity chromatography around 115 kDa that was probed with the P3 sequence (Figure 6). This band is of a different molecular weight that previously thought, but is specific to the P3 sequence and is present in previous SDS-PAGE gels.

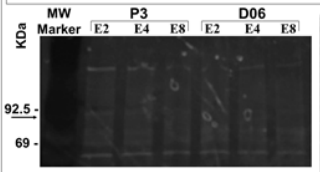

Figure 3. One specific band of 90 kDa appear in the presence of P3 but not D06 DNA

Figure 5. UniProtKB/Swiss-Prot database entry for UBF. UBF helps recruit RNA polymerase I, promoting rRNA transcription.

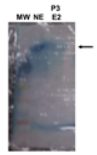

Figure 6. Southwestern blot of unpurified nuclear extract (NE) and protein purified through DNA affinity chromatography (P3 E2) probed with P3 sequence. A band is seen at approximately 115 kDa in both NE and P3 E2 that is specific for the P3 sequence.

Figure 4. Representation of data analyzed in Scaffold. (A) Results from LC-MS/MS shows UBF as the only protein present in both bands (P3 E2 and E4) with the correct molecular weight. (B) Scaffold viewer showing specific amino acid sequences that were found in LC-MS/MS, verifying presence of UBF in the samples.

V. Future Directions

Immediate Future - Two Options

- Analyze band at 115 kDa found in Southwestern blot
- Further purify extract prior to using DNA affinity chromatography
- Set up a yeast one-hybrid system to identify the protein of interest

Long Term

- Explore the biochemical properties of the protein
  - Confirm binding to the P3 region of the Cd4 promoter
  - Explore the secondary and tertiary structures of the protein

References

Gadgil, H., Luis, J.A., Jarrett, H.W. 2001. Review: DNA Affinity Chromatography of Transcription Factors. *Analytical biochemistry*. 290, 147-178

Sarafova, S., Siu, G. 1999. Control of CD4 gene expression: connecting signals to outcomes in T cell development. *Brazilian Journal of Medical and Biological Research*. 32: 785-803

Sarafova, S., Siu, G. 2000. Precise arrangement of factor-binding sites is required for murine CD4 promoter function. *Nucleic Acids Research*. Vol. 28 No. 14 2664-2671

Wada, T., Watanabe, H., Kawaguchi, H. 1995. DNA Affinity Chromatography. *Methods in Enzymology*. 254: 595-604

Acknowledgements

This research was made possible by Merck/AAAS Biochemistry Internship Program, Sigma Xi Grants-in-Aid of Research, and the Davidson Biology Department. We thank Karen Bernd, Karen Bohn, Doug Golann, Cindy Hauser, Karmella Haynes, Barbara Lom, Jeffrey Myers, Erland Stevens, Gary Surdel, and Peter Surdel.

The resolution of a mobile double Holliday junction by TopoIIIα & Blm

Jody L Plank and Tao-shih Hsieh
Department of Biochemistry; Duke University Medical Center; Durham, NC

Introduction

The double Holliday junction (dHJ) is a central intermediate of homologous recombination. Szostak et. al. postulated that the digestion of this structure by endonucleases would give rise to gene conversion events either with (crossovers, CO) or without (non-crossovers, NCO) the exchange of sequences flanking the original break site. However, in both yeast and mouse meiosis, the generation of crossover and non-crossover products has been shown to be distinctly different processes, not the differential digestion of a common intermediate. One of the proposed mechanisms for the generation of NCO products is the collapse of smaller dHJ's by topoisomerase III (topoIII) partnered with a recQ helicase.

In higher eukaryotes, there are two isoforms of topoisomerase III, α and β, and multiple recQ helicases. Of the five recQ helicases in humans, BLM, WRN, and RecQ4 have all been implicated in syndromes involving genetic instability and susceptibility to a wide range of cancers. In *Drosophila* there are three recQ helicases: Blm, RecQ4, and RecQ5. Flies mutant for DmBlm show elevated mitotic recombination, nondisjunction and chromosome loss, and are nearly sterile, recapitulating many of the features of BLM deficiency in humans. There are no known disorders associated with mutations in TopoIIIα or β, although mutations in TopoIIIα are lethal in mice and *Drosophila*, while deletion of TopoIIIβ results in adult mice with reduced fertility and an increased incidence of tumors.

With hTopoIIIα, hBLM can resolve a small synthetic dHJ. This substrate is constructed from two oligonucleotides that are annealed and ligated to form a dHJ separated by 14bp, with short duplexes outside of the junctions terminated by hairpin structures. The HJ's in this substrate are necessarily immobile, meaning that any migration of a HJ will generate ssDNA. Because of the short distance between the HJ's, the two ssDNA circles that compose the substrate only possess a linking number of two, making resolution via random strand passage events feasible. To rigorously determine if topoIII and recQ helicases are capable of resolving a dHJ and to better understand the mechanism by which any enzyme processes these structures, a new dHJ containing substrate is needed which better mimics the endogenous intermediate.

Synthesis of a larger, topologically constrained double Holliday junction substrate (DHJS) with mobile junctions

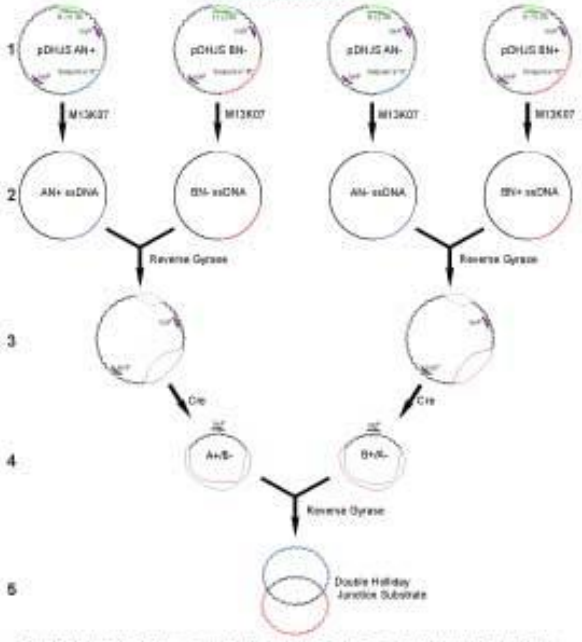

The substrate is derived from four plasmids, containing tandem loxP sites and differing with either sequence A or B with the H-origin in both the plus and minus orientations for each (1). Using the helper phage M13K07, ssDNA circles are expressed (2), purified, mixed, and linked using reverse gyrase to yield a large heteroduplex intermediate (3). The small heteroduplexes were excised utilizing Cre recombinase and the loxP sites flanking the AxB bubble (4). The small heteroduplexes are linked together with reverse gyrase to yield the double Holliday Junction substrate (5). Please note that this illustration is not to scale.

Digestion of the DHJS by T7 Endonuclease I is consistent with the predicted structure of the DHJS

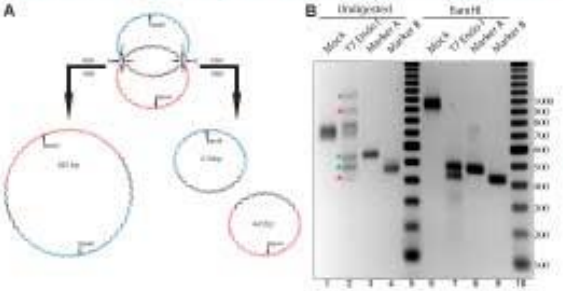

A) Partial digestion of the DHJS substrate by T7 Endonuclease I can proceed by two different pathways. If the HJs of a given molecule are cut in a perpendicular fashion, as shown in the right pathway, then the products of the reaction are predicted to be two smaller DNA circles, 440bp and 416bp. If both HJs of a given molecule are digested in a parallel fashion, as shown in the left pathway, then the expected product of the reaction would be a large DNA circle 856bp in size.
B) T7 Endonuclease I digests the DHJS in the predicted fashion. A DNA size marker was run in lanes 5 and 10, with the size of the bands denoted to the right of the gel in base pairs. ◦ Denotes the circular DNAs predicted in panel A. ▪ denotes bands corresponding to the linearization of the circles by T7 endo I, the other bands are presumed to be reaction intermediates.

The Holliday junctions are near the ends of the homologous region

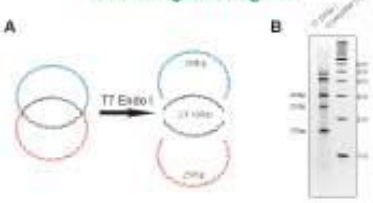

A) Complete digestion of the DHJS substrate by T7 Endonuclease I will not only cut the HJs, but will cleave the resulting circles a second time opposite the nick left behind from the first cut. With the predicted structure of the DHJS, this would result in four linear DNAs of the indicated sizes.
B) The experimentally determined sizes of the linear bands resulting from this digest correlate well with the predicted sizes of the fragments. The experimentally determined sizes of the bands are shown to the left of the gel, while the size standards are listed to the right of the gel in base pairs.

TopoIIIα & Blm resolve the DHJS, and this activity is specifically stimulated by RPA

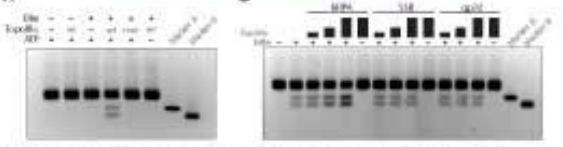

A) Resolution products are detected when both TopoIIIα and Blm are present in the reaction. When an active site mutant, TopoIIIα (Y356F), is substituted for wildtype TopoIIIα, no resolution products are detected, and when ATP is omitted from the reaction buffer, no resolution products are detected.
B) Human RPA stimulates the resolution activity of TopoIIIα & Blm, but other single-stranded DNA binding proteins do not. RPA has previously been shown to stimulate HELIM helicase activity on longer substrates.

TopoIIIα, Blm & RPA resolve the DHJS through convergent migration of the Holliday junctions

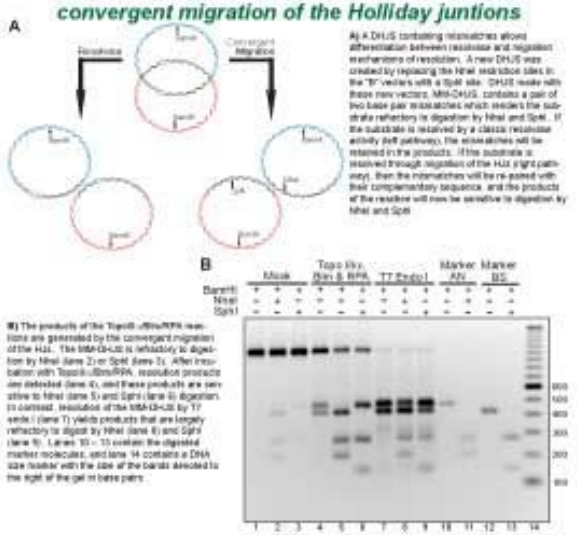

A) A DHJS containing mismatches allows differentiation between resolution and regression mechanisms of resolution. A new DHJS was created by replacing the NheI restriction sites in the "B" vectors with a SphI site. DHJS made with these new vectors, MM-DHJS, contains a pair of two base pair mismatches which renders the substrate refractory to digestion by NheI and SphI. If the substrate is resolved by a classic resolvase activity (left pathway), the mismatches will be retained in the products. If the substrate is resolved through migration of the HJs (right pathways), then the mismatches will be re-paired with their complementary sequence, and the products of the resolvase will now be sensitive to digestion by NheI and SphI.
B) The products of the TopoIIIα/Blm/RPA reactions are generated by the convergent migration of the HJs. The MM-DHJS is refractory to digestion by NheI (lane 2) or SphI (lane 3). After incubation with TopoIIIα/Blm/RPA, resolution products are detected (lane 4), and these products are sensitive to NheI (lane 5) and SphI (lane 6) digestion. In contrast, resolution of the MM-DHJS by T7 endo I (lane 7) yields products that are largely refractory to digest by NheI (lane 8) and SphI (lane 9). Lanes 10 – 13 contain the digested marker molecules, and lane 14 contains a DNA size ladder with the size of the bands denoted to the right of the gel in base pairs.

Conclusions

We have synthesized a novel substrate that recapitulates many of the features of endogenous double Holliday junctions. The distance between the junctions are on the order of the size of NCO products generated in both yeast and mouse meiosis, and creates a linking number of ~30, providing a more rigorous test for enzymes that might resolve this structure through convergent migration of the HJs. This substrate allows for the migration of the HJs (in one direction) without the generation of ssDNA, and its circular nature provides the same topological constraints that endogenous dHJs are likely to possess. In addition to these features, the method by which the DHJS was created allows for tremendous flexibility in the creation of new substrates.

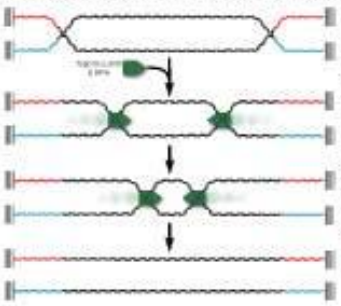

When this substrate is incubated with TopoIIIα and Blm helicase, it is resolved in a NCO fashion. This activity is specifically stimulated by RPA, a protein that had previously been shown to stimulate HELIM helicase activity. These proteins resolve the DHJS through convergent migration of the HJs, reducing the linking number of the two DNA circles that comprise the DHJS from ~30 to 0. Given the established protein-protein contacts that have been discovered between BLM and TopoIIIα and BLM and RPA, it is likely that these three proteins form a complex to migrate a HJ without the accumulation of topological stress, as shown to the left.

Acknowledgements

We would like to thank the members of the Hsieh lab for many critical discussions that went into the development of this work. I would also like to thank Carrie Reardon for the generation of the huge amounts of ssDNA required to make this substrate. This work was supported by the NIH (GM29085) and by a NSF predoctoral fellowship.

Palaeodistribution of *Polylepis* forests in the Andes

Adèle Kuentz[1,2], Marie-Pierre Ledru[2], Jean-Claude Thouret[3]

1/ Laboratoire CERAMAC, Maison de la Recherche, Université Blaise Pascal, Clermont-Ferrand, France, & Institut Français des Etudes Andines, La Paz, Bolivia.
2/ IRD, UR032 Great Ice, France. 3/ Laboratoire Magmas et Volcans UMR 6524 CNRS, Université Blaise Pascal, Clermont-Ferrand, France.

INQUA 2007 CONGRESS
Cairns, Australia
Saturday 28 July - Friday 3 August 2007

Biodiversity Conservation and the Relevance of Quaternary Palaeoecology session

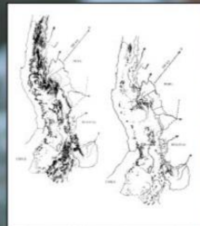

Figure 1: potential distribution of *Polylepis* (left) and present distribution of *Polylepis* (right) (Fjeldsa and Kessler, 1996).

Polylepis forests shows a high degree in biodiversity. They have been stongly reduced for the past decades. (fig.1) [15].

What are the impacts of climate change and deforestation on its distribution today?

Pollen records were reviewed to understand their past development and their modern distribution. We aim to contribute to their preservation in the perspective of a climate change and an increase of human pressure in the tropical Andes for the coming years and act in policies for their conservation.

Two examples of *Polylepis* patterns. Dense altitudinal patches with large trees and rich undergrowth (picture above). Monospecific altitudinal patches of forest scattered in dry environments with poor undergrowth (picture below).

Modern distribution

Polylepis forests are found at high elevation in the Andes where they expand today from Venezuela to Argentina (from 9°N to 32°S). Three types of *Polylepis* habitats can be observed: 1) *Polylepis* trees represent a component of the timberline of the Andean rain forest on the eastern slope of the Andes, 2) *Polylepis* trees form dense altitudinal patches with big trees and a rich undergrowth, 3) *Polylepis* trees form monospecific altitudinal patches of forest scattered in dry environments with a poor undergrowth. Microclimate or human pressure influences (Table 1)?

Arguments against a human pressure on the distribution of *Polylepis*	In favor of a human pressure
Polylepis patches are found in specific habitats	Not only in specific habitats
Some woodlands have survived near villages	Man can maintain patches near their habitation and destroy other patches for pasture
Polylepis can well re grow after a cut down	Fire is a slow but continuous damage
Poor human populations in these high altitudes	Fire can extend over wide area and generated by one person
Palynological studies show that *Polylepis* did not expand during the last 10 000 yr BP	
	Polylepis patches are located in sites were fire can't extend
	Polylepis is met in sites were there is no fire and no pasture
	Biogeographic studies show that *Polylepis* was more extended during the last interglacial period when human was less present

Table 1: Description of the facts against and in favor a human pressure on the distribution of *Polylepis* (after Fjeldsa & Kessler, 1996).

Methods

Changes in *Polylepis* pollen frequencies are characterized for the last 20,000 years BP. from published palynological records. All radiocarbon dates were calibrated using Calib501 [18] (Fig. 2).

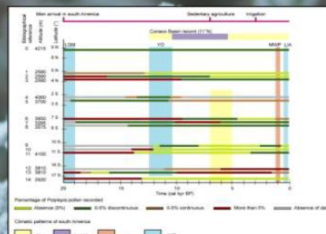

Figure 2 : variation of *Polylepis* spectrum in various pollen diagrams, principal climatic patterns of south America and human pressure

Production and transport of the pollen

***Polylepis* pollen frequencies of even less than 1% were recovered in a distance of less than 1 km from the *Polylepis* woodland [19].**

Bibliographical Reference (see bibliography)	Study site	Latitude	Longitude	Altitude (m)	Current position of *Polylepis* woodlands (altitude in m)	Significance of *Polylepis* variation in pollen diagram
0	Laguna verde alta	8°51'N	70°52'W	4215		
1	Lake Fuquene Fuquene II	5°27'N	73°46'W	2580	2300-3500	*Polylepis* forest are higher than the core site. Increase of *Polylepis* = colder
2	Lake Fuquene Fuquene VII	5°27'N	73°46'W	2580	2300-3500	
3	Lake Fuquene Fuquene III	5°27'N	73°46'W	2580	2300-3500	
4	Laguna Pallcacocha	2°45'S	79°13'W	4060		Fires affect *Polylepis*, dry seasons and warm temperatures favor *Polylepis* growth
5	Laguna Chorreras	2°45'S	79°10'W	3700		
6	Laguna La Compuerta	7°30'S	78°36'W	3950		
7	Laguna de Chochos	7°38'S	77°28'W	3285	2800-3500	Increase of *Polylepis* = events dry and warm with possibles short humid periods. fires
8	Laguna Baja	7°42'S	77°32'W	3575	2300-3500	
9	Laguna Huatacocha	10°45'S	76°35'W		3300-4300	
10	Laguna Rio Blanco	10°45'S	76°20'W		3300-4300	
11	Laguna Junin	11°S	76°W	4100	3300-4300	
12	Lake Titicaca	16°S	68°5'W	3810		Increase *Polylepis* = Diminution available moisture
13	Lake Titicaca	16°S	68°5'W	3810		
14	Cerro Sillajhuay	17°5S	64°43'W	2920		Increase of *Polylepis* and *Podocarpaceae* = increase in moisture

Table 2: location of the sites from which diagrams are studied, classed by latitude from north to south. Current position and description of the *Polylepis* woodlands, significance of *Polylepis* variation in pollen diagram (according to each author).

Results

Differences in *Polylepis* signals are observed according to geographical position and climatic condition for the past 20,000 years. 1) Some forests have been reduced or disappeared [sites 1,2,3 (latitude 5°27N),10,11,14 (10°45S, 11°S, 17°5S respectively]. 2) Some forests expanded and stabilized [5 (2°45S),12,13 (16°S)]. 3) No changes were ever recorded in two of them [0 (8°51N), 8 (7°42S)] while others recorded successively expansion/regression [6,7,9 (7°3, 7°3, 10°45 respectively)].

Although datations and resolution of the pollen records are strongly heterogeneous, we observe that ruptures in *Polylepis* frequencies do not appear simultaneously even when sites recorded are very nearby geographically. An explanation is that the *Polylepis* pollen signal is very local and the forests never widely expanded over a single territory. All the paleoenvironmental records are located in the modern elevation range of *Polylepis* woodlands distribution and an increase in *Polylepis* pollen frequencies is sometimes associated with opposite climatic patterns (Table 2).

To compare and relate variations of *Polylepis* frequencies with climatic parameters it is necessary to know the location of the core and of the closest *Polylepis* woodlands: for example if the core is located at a lower elevation than the forest, *Polylepis* frequencies will increase when the vegetation belt shift downslope under colder climate (Fuquene lake). At laguna de Chochos the opposite situation is observed: the coring site is located above the *Polylepis* forest.

Human pressure can strongly influenced the regression of the *Polylepis* in the Andes and fire is able to damage the vegetation at a long-term. For example, at Lake Junin charcoal concentration increased together with a decrease in *Polylepis* pollen frequencies, and at Lake Fuquene *Polylepis* pollen are observed for the past 5 MA but are rare or not recorded today.

Conclusion

The evolution of the Andean *Polylepis* forests does not show a uniform pattern of evolution since the last 20,000 years. All the sites below 3000 m show a strong regression of *Polylepis* forests since the last 20,000 yrs. These sites could be considered as a refugia during the last glacial maximum that progressively expanded upslope during the Holocene.

Modern distribution of the *Polylepis* forests results of combined factors such as a restricted ecology, a poor reproduction (a lot of steriles seeds), his distribution reduced in refuge during the glaciation, climatic variations and human pressures. Multidisciplinary projects are developed to increase the number of informations on the paleo ecology and ecology of the Andean *Polylepis* forests.

Young plants at the edge of the patch are exposed to the high radiation in the day strong cold in the night and fire put by farmers. That's why the forests extend with difficulty. 4000 m of elevation. Cordillera Vilcabamba, Peru.

Adult *Polylepis* arch can reach 7 meters high. 4000 m of elevation. Cordillera Vilcabamba, Peru.

The hypothesis wich explains the high number of bark layers is about protection the arbol from cold and fire. 4000 m of elevation. Cordillera Vilcabamba, Peru.

Inflorescence of *Polylepis* besseri southwestern part of the Nevado Coropuna, 4600 m, Peru. Size of the flower ca. 3 mm.

An example of specific biodiversity : *Cinclodes aricomae* is an ultra dependent of *Polylepis* forests, only a few hundred pairs of this bird exists in the world. 4000 m of elevation. Cordillera Vilcabamba, Peru.

Mean references with the number corresponding in table 2 and figure 2

7. Bush, M. B. et al., (2005) Journal of quaternary science. 20, (7-8), 703-714.
15. Fjeldsa, J. & Kessler, M., (1996). Conserving the Biological Diversity of *Polylepis* Woodlands of the Highland of Peru and Bolivia. Copenhagen, NORDECO, 214p.
16. Graf, K., (1981) Journal of Biogeography. 8, 353-368.
12. Hanselman, J. et al., (2005) Journal of quaternary science. 20, (7-8), 663-670.
9,10,11. Hansen, B. et al., (1984) Geological Society of America Bulletin. 95, 1454-1465.
6. Hansen, B. & Rodbell, D.T., (1995) Quaternary Research. 44, 216-227.
4,5. Hansen, B. et al., (2003) Palaeogeography, Palaeoclimatology, Palaeoecology. 194, 79-108.
19. Kuentz, A. et al., (2007) Journal of Biogeography. Published article online, 29 May 2007, doi:10.1111/j.1365-2699.2007.01728.x
17. McCormac, F. G. et al., (2004) Radiocarbon. 46, 1087-1092.
14. Mourguiart, P. & Ledru, M.P., (2003) Geology. 31, (3), 195-198.
13. Paduano, G. et al., (2003) Palaeogeography, Palaeoclimatology, Palaeoecology. 194, 259-279.
0. Rull, V. et al., (2005) Quaternary Research. 64, 308-317.
3. Van der Hammen, T. & Hooghiemstra, H., (2003) Global and Planetary Change. 36, 181-199.
1,2. Vriel, R. et al., (2000) Quaternary Science Reviews. 19, 1621-1635.
8. Weng, C. et al., (2006) Quaternary Research. 66, 87-96.

IRD Institut de recherche pour le développement — GREAT ICE — IFEA Institut Français d'Etudes Andines — Université Blaise Pascal — UM2 Université Montpellier 2 Sciences et Techniques — ISE Montpellier

Identification of the Cell of Origin for Wnt Pathway-Associated Medulloblastoma

Yanxin Pei and Robert Wechsler-Reya
Department of Pharmacology & Cancer Biology, Duke University Medical Center, Durham, NC.

ABSTRACT

Wnt pathway mutations have been found in cerebellar medulloblastoma, the most common malignant brain tumor in children. However, the cell type that is transformed by aberrant Wnt signaling remains unknown. Our goal is to identify this cell and use it to develop models for Wnt pathway-associated medulloblastoma. To this end, we are developing transgenic mice that will allow us to label Wnt-responsive progenitors in the cerebellum. These cells will be isolated and tested for their ability to be transformed by Wnt-pathway activation. In addition, many human medulloblastomas express the transcription factor Neurogenin-1 (Ngn1), raising the possibility that Ngn1+ cells might represent a cell of origin for these tumors. We have used the Ngn1 promoter to drive expression of β-catenin (a Wnt pathway mediator) in vivo. These mice have smaller cerebella and exhibit defects in cerebellar development. Ongoing studies will determine whether prolonged activation of Wnt signaling in Ngn1+ cells is sufficient to cause medulloblastoma. Finally, we have observed that CD133+ neural stem cells proliferate in response to Wnt pathway activation in vitro and following injection into the cerebellum. In future studies we will test whether these cells can form tumors following transplantation. These studies will provide important insight into the cellular and molecular mechanisms of medulloblastoma.

BACKGROUND

Medulloblastoma is the most common malignant brain tumor in children. It has been divided into two major subtypes based on histological and molecular characteristics: "classic" medulloblastomas and "desmoplastic" medulloblastomas. The cell of origin is not clear for either subtype but some studies suggest that the former may originate from multipotent precursors in the ventricular zone of the cerebellum, while the latter may originate from granule cell precursors in the external germinal layer (EGL). Recent studies have suggested that the Sonic hedgehog-Patched signaling pathway plays a critical role in regulating the proliferation of granule cell precursors and is also a major target of mutation in desmoplastic medulloblastomas. However, the pathogenesis of classic medulloblastomas remains unknown. Some findings suggest that the Wnt-β-catenin signaling pathway is activated in a subset of these tumors. Understanding of the role of Wnt pathway in tumor information may shed light on the etiology of classic medulloblastomas.

Wnts are secreted proteins that have been implicated in many developmental processes including cell fate specification, proliferation and differentiation. Wnts activate target genes through β-catenin, one of the key downstream effectors in the Wnt signaling pathway. Activating mutations in β-catenin Exon3 have been identified in 5-10% of sporadic medulloblastomas. In addition, mutation of Wnt1 results in the loss of mid-hindbrain boundary, from which the cerebellum arises. Thus, Wnt-β-catenin signaling plays a critical role in the development of cerebellum and formation of medulloblastoma.

Although Wnt-β-catenin signal activation can induce cell proliferation and tumor formation, the role is cell-type dependent. Our goal is to identify the cell of origin for Wnt signaling pathway in the formation of medulloblastoma.

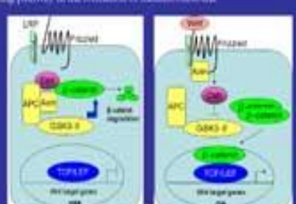

Wnts signaling pathway. Wnts activate expression of target genes through β-catenin which is an essential component in the Wnt pathway. In the absence of Wnt signaling, β-catenin is in a complex with Axin, APC and GSK3-β, and gets phosphorylated and subsequently degraded by protoosomes. In the presence of Wnt signaling, β-catenin is uncoupled from the degradation complex and translocates to the nucleus, where it binds TCF/LEF transcription factors, thus activating target genes.

1. Expression of Neurogenin I (NgnI)

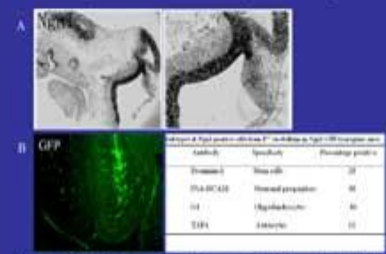

Expression of Ngnl in a subset of cerebellar progenitors.

2. Generation of mice in which β-catenin is activated in Ngn I positive Cells

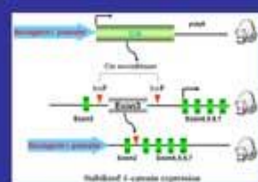

Stabilized expression of β-catenin under the control of of Ngnl promoter.

3. E18 Cerebellum in Ngn1-βcat* Mice

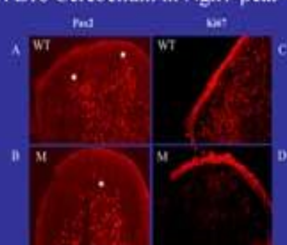

Migration and proliferation of cerebellum.

4. Generation of mice in which β-catenin is activated in Neurogenin-1^{+} Cells

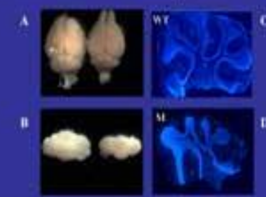

Ngn1-βcat* mice have defects in cerebellar size and structure.

5. Stem Cell Property of CD133 Positive Cells

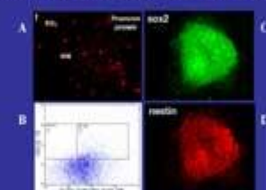

CD133 is expressed in cerebellar stem cells.

6. CD133 Positive Cells Proliferate in Response to Wnt Signaling

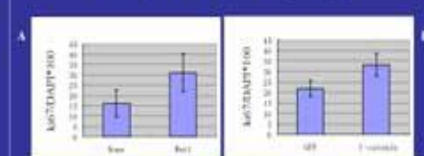

Proliferation of CD133 positive, Lineage negative cells (CD133+, Li-).

7. Generation of BAT-CreER Mice to Track the Fate of Wnt-Responsive Cells

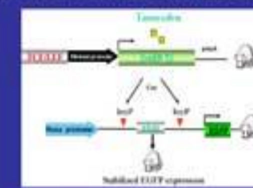

Stabilized expression of EGFP under the control of of TCF/LEF promoter.

8. Bat-CreER Activation by β-catenin in 293T Cells

Cre Protein Expression in 293T Cells.

CONCLUSIONS

- Ngnl is expressed in cerebellar progenitors during embryonic and early postnatal development.
- Overexpression of β-catenin in Ngnl positive cells reduces the size of the cerebellum and causes defects in interneuron migration, but does not cause tumors (so far ...)
- Wnt1 protein and β-catenin virus can induce the proliferation of CD133 positive cerebellar stem cells.
- β-Catenin-infected stem cells are now being transplanted into the cerebellum to examine their tumorigenic potential.
- BAT-CreER mice will allow lineage-tracing of Wnt responsive cells in the cerebellum, and may identify new candidates for the cell of origin of Wnt-associated medulloblastoma.

ANALYSE COMPARATIVE DES METHODES ANALYTIQUES DE DOSAGE DES PREPARATIONS D'ANTICANCEREUX EN UNITE DE RECONSTITUTION CENTRALISEE

C. RENZULLO, C. PAILLET, C. PIVOT

Unité de Préparation Centralisée Pharmaceutique (UPCP)
Hôpital Edouard. Herriot 5, place d'Arsonval - 69437 LYON Cedex 03

INTRODUCTION

Dans l'objectif de garantir la qualité des préparations d'anticancéreux, les pharmaciens de l'UPCP de l'Hôpital Edouard Herriot (Hospices Civils de Lyon) ont fait le choix d'acquérir un équipement pour le contrôle analytique des préparations d'anticancéreux.

Ainsi, plusieurs critères de choix ont été définis afin de réaliser une analyse comparative des différentes méthodes applicables à ce domaine d'activité que sont : la **Chromatographie Liquide Haute Performance** (HPLC), la **Chromatographie sur Couche Mince à Haute Performance** (HPTLC) et la **Spectroscopie InfraRouge à Transformée de Fourier** (IRTF).

MATERIEL ET METHODE

A) REDACTION DU CAHIER DES CLAUSES TECHNIQUES :

Définition de critères de choix pour l'acquisition d'un matériel de chromatographie ou de spectrométrie permettant l'analyse qualitative et quantitative des molécules anticancéreuses (cytotoxiques et anticorps monoclonaux) dans les préparations effectuées quotidiennement par l'UPCP pour les services pratiquant l'oncologie et l'onco-hématologie

B) ANALYSE COMPARATIVE des 3 méthodes disponibles actuellement sur le marché selon :

- les données fournies par les industriels lors d'entretiens en tête-à-tête et de visites des installations sur site.
- une cotation en 4 niveaux : très défavorable (--), défavorable (-), favorable (+) et très favorable (++)

RESULTATS

A) DEFINITION DES CRITERES DE CHOIX PRINCIPAUX

1) GENERAUX :

- Facilité de mise en œuvre initiale, en routine et en urgence
- Assistance à la mise en route
- Documentation technique
- Besoin en formation des utilisateurs
- Coût global (équipement, formation, maintenance, consommable)

2) TECHNIQUES :

- Temps d'acquisition du résultat ≤ 5 minutes
- Volume d'échantillon prélevé minimum
- Édition d'un bulletin d'analyse pour chaque dosage
- Manipulations humaines limitées
- Gestion rigoureuse et efficace des effluents et déchets
- Description des consommables

3) FONCTIONNELS :

- Équipement avec encombrement le plus limité possible
- Soutien technique du fournisseur (hotline...) sur le long terme
- Adaptation possible au dosage de nouvelles molécules dans les meilleurs délais
- Logiciel informatique convivial d'utilisation simple avec traçabilité et archivage des données en vue d'une ré analyse ultérieure

B) ANALYSE COMPARATIVE

TECHNIQUE / CRITERES	IRTF	HPLC	HPTLC
Délais d'analyse	++	+	-
Meilleure offre (acquisition + formation)	++	-	+
Facilité de mise en œuvre y compris en urgence	+	-	-
Encombrement minimal	++	+	-

DISCUSSION - CONCLUSION

La Spectroscopie InfraRouge à Transformée de Fourier (IRTF) semble combiner les avantages des techniques physiques (rapidité et simplicité) permettant d'assurer la vérification avant la dispensation des préparations même en situation d'urgence et ceux des techniques chromatographiques plus compliquées à mettre en œuvre (spécificité et précision). A ce jour, une trentaine de molécules anticancéreuses peuvent être dosées avec l'IRTF, y compris des anticorps monoclonaux. Le volume de l'échantillon reste à optimiser. Notre choix s'oriente sur l'acquisition de cette méthode pour améliorer la performance de nos contrôles - qualité en routine au sein de notre Unité de Préparation Centralisée Pharmaceutique.

Sixièmes Journées de la Société française de Pharmacie Oncologique – Nice – 11 et 12 octobre 2007

LPED
Laboratoire
Population
Environnement
Développement
www.lped.org

La subvention des médicaments antipaludiques favorise-t-elle une plus grande équité d'accès aux soins ? L'exemple du recours aux soins à Dakar, Sénégal.

G. Koné[2,1], M. Audibert[3], R. Lalou[1], A. Mbaye[2], S. Dos santos[1]
1. LPED – IRD/Aix-Marseille Université, 2. Université Cheikh Anta Diop de Dakar (UCAD),
3. CERDI - CNRS/Université d'Auvergne.

DEFINITION

A Dakar, la densification du peuplement, notamment dans les quartiers périphériques, et les inondations de la dernière décennie (1996, 2005 et 2008) ont favorisé une augmentation localisée des niveaux de transmission du paludisme (résurgence d'une infection endogène). En outre, le paludisme constitue dans de nombreux quartiers dakarois le motif de consultation de plus de 35% des recours aux soins.

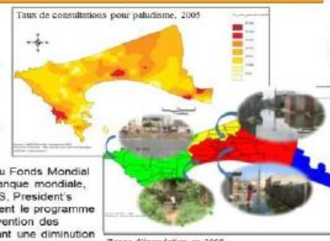

Zones d'inondation en 2008

Le Sénégal a remporté trois rounds du Fonds Mondial depuis 2001. D'autres partenaires (Banque mondiale, Banque Islamique, BAD, USAID, OMS, President's Malaria Initiative) soutiennent également le programme de lutte contre le paludisme et la subvention des médicaments (depuis 2006), permettant une diminution progressive du fardeau du paludisme pour la population cible (femmes enceintes et enfants de moins de cinq ans).

Objectif

Notre objectif est de vérifier si les mécanismes de subvention du traitement et de prévention du paludisme ont permis de lever la barrière financière du recours aux soins de santé moderne des enfants de 2 à 10 ans en cas d'épisode fiévreux, et de favoriser la fréquentation des établissements de santé par les ménages les plus pauvres.

Hypothèses

Nous posons l'hypothèse qu'en situation d'incertitude du diagnostic et de la gravité de la maladie :

- **l'automédication est la stratégie privilégiée des ménages pauvres ; les ménages riches sont davantage susceptibles de bénéficier des médicaments subventionnés.**
- **Dans les quartiers ayant une forte population riche (influence sociale) ou présentant des risques environnementaux élevés (réduction de l'incertitude), la fréquentation des formations de santé est plus élevée quel que soit le niveau économique du ménage.**

METHODES

Une enquête ménages réalisée en 2008 à Dakar : 50 quartiers ont été tirés et 2.952 ménages comprenant 28. 698 individus dont 7.413 enfants de 2 à 10 ans, ont été enquêtés.

Le cadre conceptuel fourni par Andersen(1995) est un outil d'analyse pour identifier et tester les relations causales entre l'accès aux soins et les facteurs individuels et contextuels (Guend, 2006).

Le modèle probit multi-niveau a été utilisé pour estimer la demande de soins. L'approche multi-niveau permet de dépasser les limites des modèles classiques (Courgeau, 2002 ; Hoen, 2007), et de prendre en compte les influences contextuelles (quartier). La variable réponse: le type de recours, comprend l'automédication (50,65% des choix), le recours hors du domicile (49,35%, avec 37,24% au public et 12,12 au privé). La demande de soins a été estimée sur le sous-échantillon de 1238 ménages ayant eu au moins un enfant malade le mois précédant le passage de l'enquêteur

RESULTATS

Le coût moyen (écarts-type) est de 825 (1202) F.CFA pour l'automédication, de 5763 (3206) F.CFA pour le recours externe public et de 5141 (3417) F.CFA pour le recours externe privé ou confessionnel.

La pratique de l'automédication est hétérogène entre les quartiers de résidence.

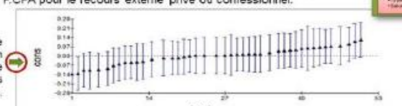

Régression Probit multi-niveau. Variable expliquée : automédication vs recours à établissement médical.

	Modèle 0 (Modèle vide)		Modèle 1 (Facteurs individuels)		Modèle 2 (Facteurs contextuels)	
	Elasticité (sd)	Z-Stat	Elasticité (sd)	Z-Stat	Elasticité (sd)	Z-Stat
Facteurs prédisposant individuel						
Niveau d'éducation de la Mère						
Aucun niveau	Référence		référence		référence	
Niveau primaire	-		0,18 (0,08)**	2,12	0,19(0,09)*	2,04
Secondaire et plus	-		[illegible]	[illegible]	[illegible]	[illegible]
Proportion des enfants de 2 à 10 dans le ménage	-		0,38(0,37)	1,66	0,37(0,27)*	1,36
Facteurs facilitant individuel						
Niveau de vie du ménage						
Très pauvres	Référence		référence		référence	
Pauvres	-		0,03(0,13)	0,25	[illegible]	[illegible]
Intermédiaires	-		-0,00(0,12)	-0,00	[illegible]	[illegible]
Riches	-		-0,30(0,14)*	-2,06	-0,24(0,10)**	-2,28
Mère ayant ou ne non une activité économique						
Non occupé	Référence		référence		référence	
occupé			0,13(0,06)**	2,02	[illegible]	3,06
Niveau de réseau social de la mère						
Faible	Référence		référence		référence	
Moyen	-		[illegible]	0,94	0,09(0,11)	0,86
Bon (fort)	-		[illegible]	[illegible]	[illegible]	3,40
Couverture sociale du ménage						
Pas de couverture sociale	Référence		référence		référence	
Dispose de couverture sociale	-		-0,21 (0,19)	1,12	[illegible]	[illegible]
Aptitude et connaissances en santé						
Niveau de culture en santé de la mère						
Faible	Référence		référence			
moyen	-		[illegible]	2,19	[illegible]	2,40
Bon (fort)	-		[illegible]	1,68	[illegible]	1,77
Facteurs contextuels						
Niveau de pauvreté du quartier						
Pauvre (class_fin_q1)	Référence				référence	
[illegible] (class_fin_q2)	-		-		[illegible]	[illegible]
[illegible] (class_fin_q3)	-		-		[illegible]	[illegible]
Offre de soins dans le quartier						
Densité d'officines de pharmacie privée						
Faible (DistPharmacie_q1)	référence		Référence		Référence	
Moyenne (DistPharmacie_q2)	-		-		[illegible]	0,88
Forte (DistPharmacie_q3)	-		-		[illegible]	1,36
Coût moyen du traitement dans le quartier (en F CFA)	-		-		[illegible]	[illegible]
Besoin de santé dans le quartier						
Niveau de risque d'inondation du quartier						
Faible (RisqInondat_q1)	Référence		référence		référence	
Moyen (RisqInondat_q2)	-		-		[illegible]	[illegible]
Elevé (RisqInondat_q3)	-		-		[illegible]	[illegible]
Proportion enfants de 2 à 10 ans ayant eu la fièvre dans le quartier	-				[illegible]	[illegible]

- Plus le ménage est riche, plus la probabilité d'utiliser les services de santé publics et privés en cas de fièvre est grande (vs l'automédication).

  Nous observons avec une autre analyse (probit multinomiale) que la plus forte pratique du recours externe dans les ménages riches concerne plutôt les structures publiques (coef.=0,14 [0,008]; z=1,62)

- Le fait de résider dans un quartier à forte population riche augmente la proba. de recourir à un service de santé externe. En outre, l'introduction d'une variable d'interaction: « niveau éco. du quartier x niveau éco. du ménage » (non présentée) indique que les ménages pauvres dans des quartiers riches utilisent davantage les structures médicales (coef.=0,39 [0,22], z=1,76).

- Plus les risques d'infection sont ressentis fortement dans le quartier et plus les ménages vont directement consulter un établissement médical.

DISCUSSION

A l'issue de cette analyse, nous observons que les enfants fiévreux issus des ménages riches consultent davantage le médecin et sont plus susceptibles de bénéficier des médicaments subventionnés fournis par les établissements publics que les enfants des familles pauvres.

Dans un contexte de forte pratique de l'automédication, la subvention des antipaludiques notamment dans les filières privées devrait favoriser l'accès à des médicaments efficaces, notamment pour les plus pauvres. Cependant, la distribution des médicaments subventionnés se heurtent encore trop souvent à des ruptures de stock et à la résistance des pharmaciens privés. En outre, les ménages pauvres pratiquent généralement une automédication à base d'antipyrétiques (traitement des symptômes).

Il ne devrait donc pas y avoir d'effets redistributifs.

Les ménages pauvres préfèrent recourir à une structure médicale publique plutôt qu'à l'automédication quand ils résident dans un quartier riche, c'est-à-dire quand l'environnement social immédiat peut influencer leurs pratiques de soins. De même, les ménages pauvres se dispensent d'automédication – pour consulter directement – lorsque l'insalubrité et les risques sanitaires associés à leurs quartiers augmentent la gravité ressentie de l'épisode morbide et diminuent l'incertitude sur le diagnostic.

Si pour les ménages riches le coût direct des soins ne constitue pas une barrière au recours externe, l'automédication leur permet d'éviter les coûts d'opportunité du transport et de la consultation médicale, qui sont plus élevés pour les actifs.

L'automédication suppose une prise de risque. Les ménages de Dakar, les pauvres comme les riches, l'assument et tentent de réduire l'incertitude qui y est associée par une meilleure information. Pour les pauvres, il s'agit de mobiliser leur capital social, pour les plus riches, ils s'appuient sur leur capital humain.

IRD Institut de recherche pour le développement

UMR 151 IRD - Université de Provence - Centre St Charles, Case 10
13331 Marseille cedex 3 - Téléphone +33 (0)4 91 10 85 18

Exemples de posters +/-

Bons

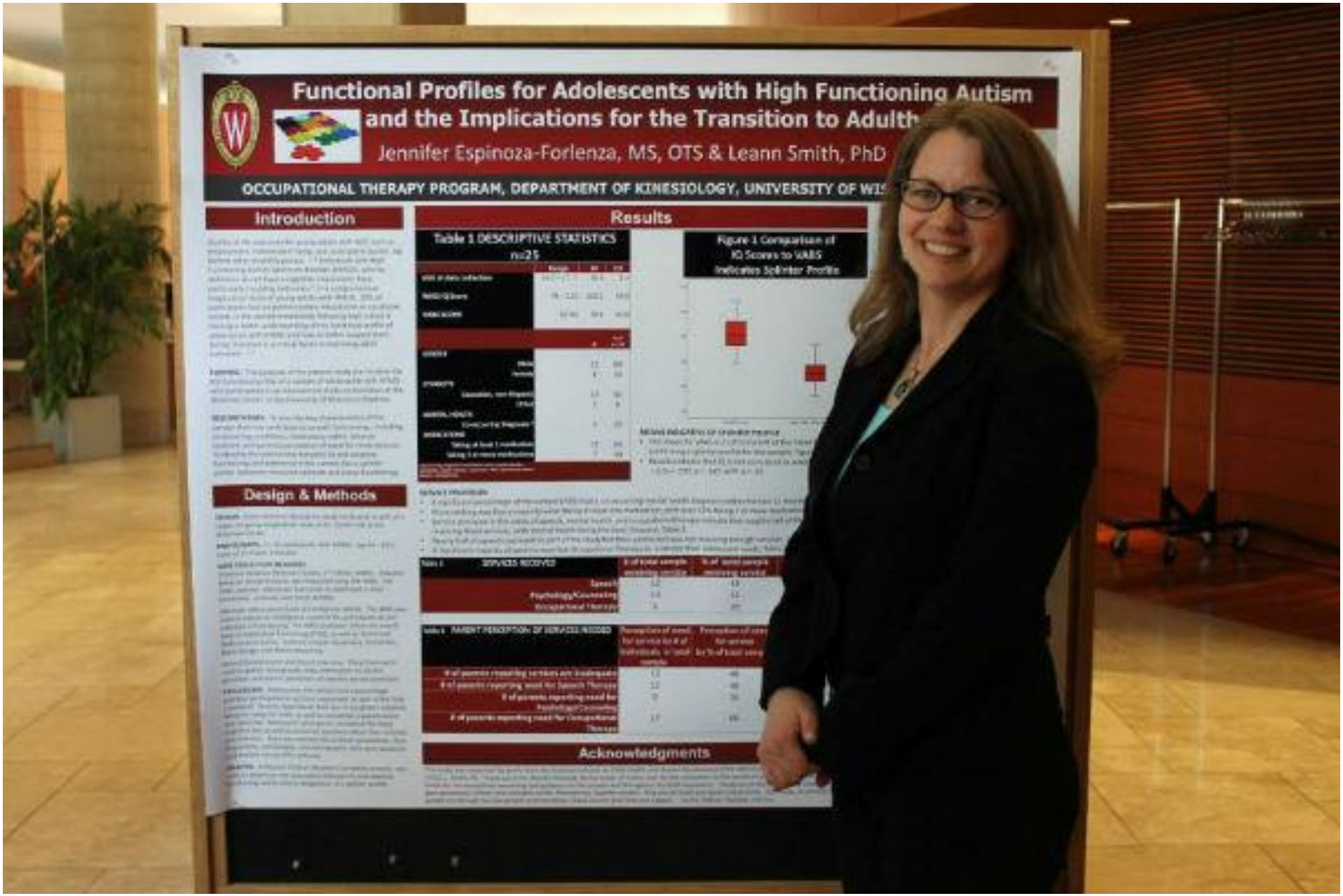
Functional Profiles for Adolescents with High Functioning Autism and the Implications for the Transition to Adulth
Jennifer Espinoza-Forlenza, MS, OTS & Leann Smith, PhD
OCCUPATIONAL THERAPY PROGRAM, DEPARTMENT OF KINESIOLOGY, UNIVERSITY OF WI
Introduction
Design & Methods
Results
Table 1 DESCRIPTIVE STATISTICS
Figure 1 Comparison of IQ Scores to VABS Indicates Splinter Profile
Acknowledgments

Distribution of Whinchats on the Eastern Moors and association with habitat and other variables

MIKE GILLETT [1] & KIM STRAWBRIDGE [2], [1] Eastern Moors Partnership volunteer,
Eastern Moors Partnership, Barbrook Cottage, Nr Owler Bar, Baslow Road, Sheffield, S17 3BQ, UK. Email: mgillett70@hotmail.com or Kim.Strawbridge@easternmoors.org.uk

Introduction

Many upland areas remain relative strongholds for Whinchats, one such area being the Eastern Moors within the Peak District. Initial surveys in 2010 identified 25 territories which were almost entirely in areas where bracken is present. The aims for 2013, which was an initial exercise to inform more detailed research in 2014, were to :

- Update the 2010 surveys
- Undertake some initial mapping to habitat and other features
- Inform and prioritise data collection needs for 2014 through analysis of some detailed data collected in 2012 from another upland site, RSPB Geltsdale
- Inform how site management plans should take account of whinchats

Methods

- A series of transect and grid square surveys were undertaken on the Eastern Moors between May and July 2013 to locate territories (singing males or pairs). From observations made, an overall assessment of the locations of territories was made
- Mapping work was undertaken in MAPINFO relating territories to habitat types and other features
- Using the data collected at Geltdale on territories and unoccupied 'control' points, logistic regression analysis was undertaken to explore the association between territory occupancy and habitat and other variables

Results from Eastern Moors

- 46 territories were identified
- almost entirely along corridors of habitat with substantial bracken cover
- nearly all following either a valley (Barbrook), a gritstone edge (White Edge), a clough or other sloping feature

Observations from Eastern Moors

- Dead bracken stands from the previous year are often the main source of perches when birds first return in Spring to establish territories
- Bracken provides an essential source of cover for offspring which fledge before they can fly
- There are some sections within the above habitat corridors without occupied territories
- Likely factors contributing to the absence of territories are :
  - the presence of too much tree cover
  - an absence of early-season perching posts (especially where dead bracken has been flattened by wind) or
  - absence of suitable long grass (or rush) for nesting
- Other factors for further research (identified from literature or proposed based on fieldwork) which may contribute to an absence of territories :
  - vegetation structure
  - nearby presence of a major road
  - nest-scale topographical features
  - damp
  - aspect, altitude
  - slope

Results from RSPB Geltsdale

Geltsdale RSPB : 50m Bracken % cover versus 50m Grass % cover for occupied and unoccupied sample sites

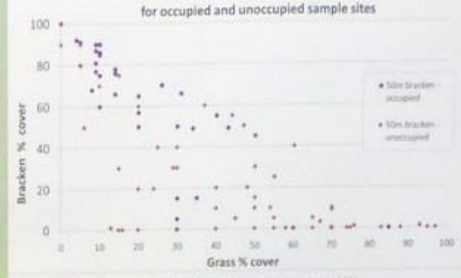

In occupied territories, median 50m % bracken cover was 66%

Aspect And Altitude

Aspect appears to have a significant influence on the altitude at which whinchats will nest. Where altitude exceeds 330m, there were no nests where aspect was W, NW, N, NE, or E. This aspect was also associated with a lower likelihood of nesting where altitude is <330m.

% Occupancy	Altitude	
Aspect	<330m	>=330m
SE, S or SW	55%	36%
W, NW, N, NE, E	50%	0%

Multivariate Analysis

In a final model from a logistic regression (LR) analysis of occupied Territories, only bracken and grass cover remained as significant variables. The c-statistic for this model was 0.78 (i.e. the model predicted occupancy/ absence correctly for 78% of survey points)

VARIABLE	ODDS RATIO	SIG.
(Bracken % – 45%) [per 1%]	1.1	0.001
Grass cover >=8% [Y/N]	30.0	0.007

A composite altitude/aspect variable did not show as significant in the LR model. This may be :

- a limitation of the simple form of the model and/or
- the result of correlations between altitude and aspect with bracken and grass cover

Further analysis may inform a more complex statistical model.

Conclusions & Discussion

- The above analyses have helped to identify areas of the Eastern Moors where :
  i) bracken removal should not be undertaken
  ii) potential conflicts with other conservation aims need to be managed (e.g. removal of trees used by corvids to predate curlew chicks, woodland creation)
- Only a small proportion of grass cover appears to be needed (at the 50m scale at least)
- Further data analysis is needed to establish the significance of aspect, altitude and slope, independent of other factors
- Future analyses should help to fine-tune understanding of habitat needs, thereby informing land management to maintain suitable habitat, and possibly suggest why whinchats are absent from some upland areas further afield

The Eastern Moors Partnership is the first time two of the UK's largest conservation charities, the National Trust and the RSPB, have collaborated to manage a site. In this case on behalf of the Peak District National Park Authority (PDNPA). Designated an SSSI, SAC and SPA, the site is to be made an even better place for people and wildlife, becoming an exemplar site for upland management. We are grateful to RSPB Geltsdale for use of their data and to Graham Thorpe for the Whinchat photo.

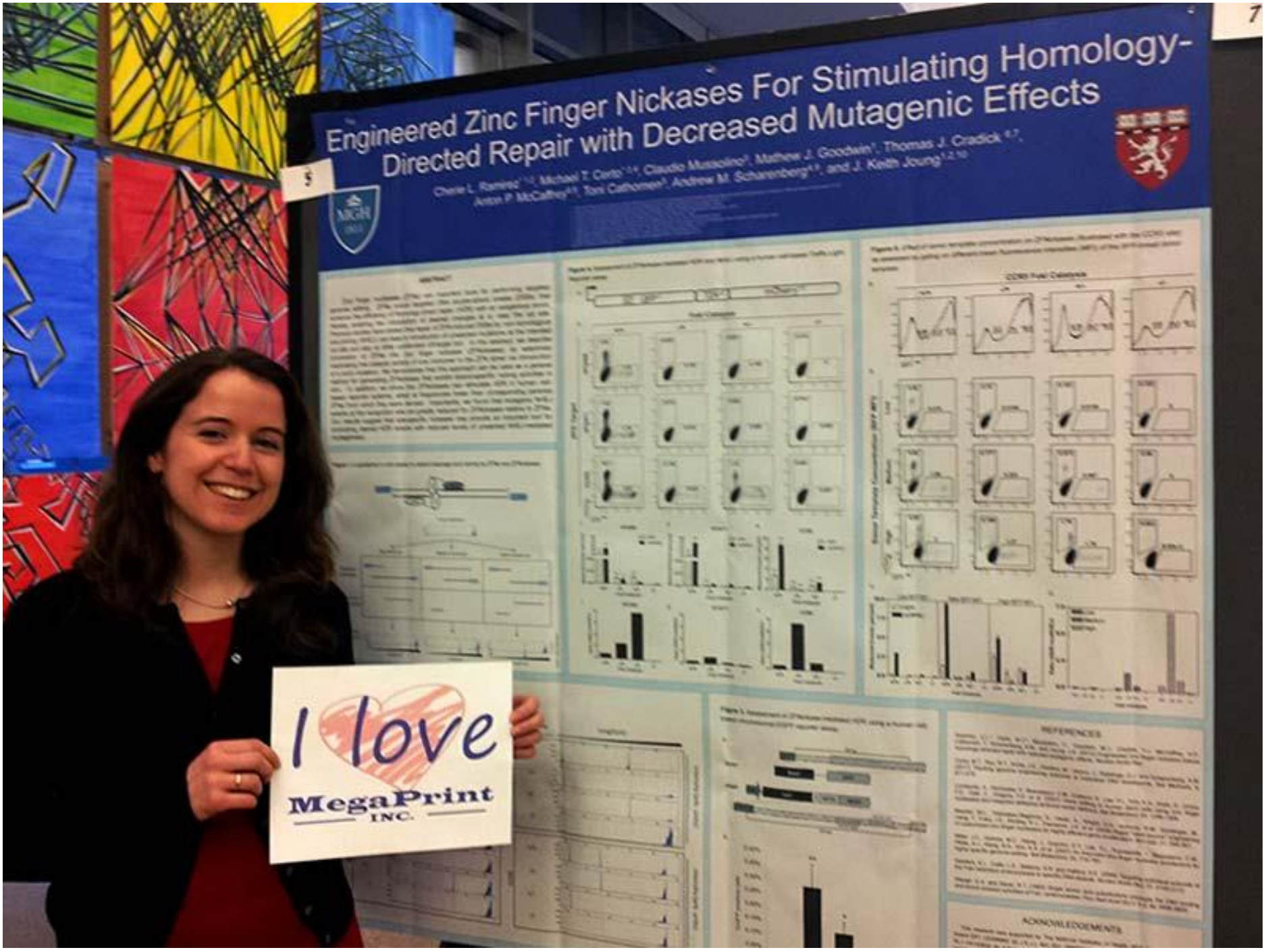
Engineered Zinc Finger Nickases For Stimulating Homology-Directed Repair with Decreased Mutagenic Effects
I love
MegaPrint
INC.

Gregory M. Crutsinger
University of Tennessee, Knoxville, TN

2006 EPA Graduate Fellowship Conference *From Discovery to Solutions: Generation Y Scientists Lead The Way*

Genotypic Diversity Predicts Community Structure and Governs an Ecosystem Process

Introduction: Accelerating declines in the earth's biodiversity have motivated extensive research on the consequences of species loss for ecosystem function. However, an often-overlooked component of biodiversity, namely population genotypic diversity, may also have wide-ranging effects on associated community structure and ecosystem processes.

...e manipulated plot-level genotypic ...altissima, or tall goldenrod. In May ...ed 63 1-m² experimental plots ...n garden, each containing 12 ..., or 12 randomly selected ...ed arthropods on every ramet in ...er the course of the growing ...unted 36,997 individuals of 136 ...Aboveground Net Primary ...the peak of the growing season.

Results: Total arthropod richness increased with plant genotypic diversity and was 27% greater in 12-genotype plots than in single-genotype plots (Fig. 2).

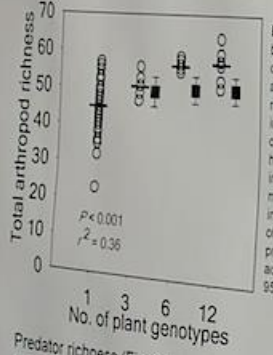

Fig. 1. Relationship between genotypic diversity and total arthropod species richness. Circles indicate plot-level observations, and horizontal lines indicate treatment means. Squares indicate the number of arthropod species predicted by simple additive models (± 95% CI).

Predator richness (Fig. 2A) and herbivore richness (Fig. 2B) also increased with increasing genotypic diversity. The effects of genotypic diversity on arthropod communities were nonadditive, or greater than predicted by summing the number of arthropod species associated with the corresponding genotypes grown in monoculture ($P < 0.01$) (Fig. 1).

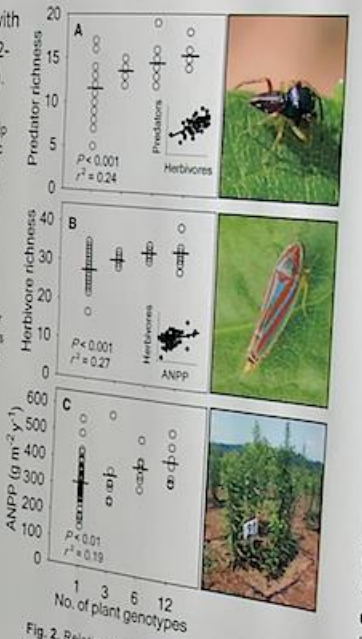

Fig. 2. Relationship between genotypic diversity and predator species richness (**A**), herbivore species richness (**B**), and ANPP of *S. altissima* (**C**). Open circles indicate plot-level observations, and horizontal lines indicate treatment means. The inset in (A) shows the relationship between herbivore species richness and predator species richness ($r^2 = 0.36$, $P < 0.001$), and the inset in (B) shows the relationship between ANPP and herbivore richness ($r^2 = 0.17$, $P < 0.001$).

We compared the standardized effect sizes (SES) of genotypic diversity to species diversity using data from the Cedar Creek LTER. The SES of plant genotypic diversity on both arthropod diversity ($SES_{gen} = 1.80$) and ANPP ($SES_{gen} = 1.33$) from our study were directly comparable to plant species diversity ($SES_{sp} = 0.93$), ($SES_{sp} = 1.35$).

Take-Home: Our results highlight the need to incorporate intraspecific variation into current ecological theory that has emphasized the importance of interspecific variation. Given the focus of conservation efforts on how the loss of species from communities affects ecosystem processes, our work suggests that the loss of genotypes from populations can no longer be overlooked.

Acknowledgements: N. Sanders, R. Dunn, A. Classen, J. Fordyce, K. Crawford, J. Hite, W. Abrahamson, J. Bailey, M. Cadotte, R. Dunn, V. Eviner, N. Gotelli, M. Johnson, J. Schweitzer, D. Simberloff, J. Williams, C. Nice, Z. Gompert

Crutsinger et al. (2006) SCIENCE 313: 966-968

...is fellow is sponsored by EPA's STAR or Greater Research Opportunities (GRO) Pro...

A Compartment Model for the Transport and Storage of Folate

Mentor: Dr. H. Frederik Nijhout Biology Department, Duke University
Tiffany J. Chen

Objectives:

- To estimate the average pool sizes of folate distributed within the plasma, the cell, and the mitochondria.
- To develop mathematical models that represent these pool sizes and mimic real bodily responses to day-to-day changes in diet and metabolism.
- To test these models against experimental data, as well as make predictions.

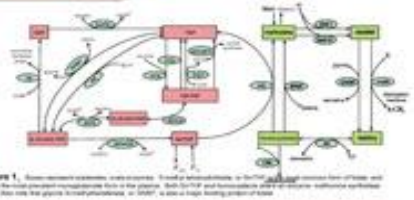

Background:

Folate, or vitamin B9, is important for the synthesis of thymidine, a pyrimidine, and purines. Deficiency in folate is associated with megaloblastic anemia, cancer, cardiovascular disease, neurological disorders, and neural tube defects in infants. Folate metabolism provides the rate-limiting step for DNA synthesis and DNA and histone methylation (Fig. 1). Reduced folate status affects these critical cellular activities and also increases the level of homocysteine, a highly reactive amino acid that is associated with cell damage. It has been shown that increased folate intake by pregnant women can help reduce the risk of infant neural tube defects, presumably due to a reduction in plasma homocysteine levels. Folate metabolism occurs within cells, but their levels are typically measured in the plasma. It is therefore critical to understand the relationship between the concentrations of folate in the plasma and the cell.

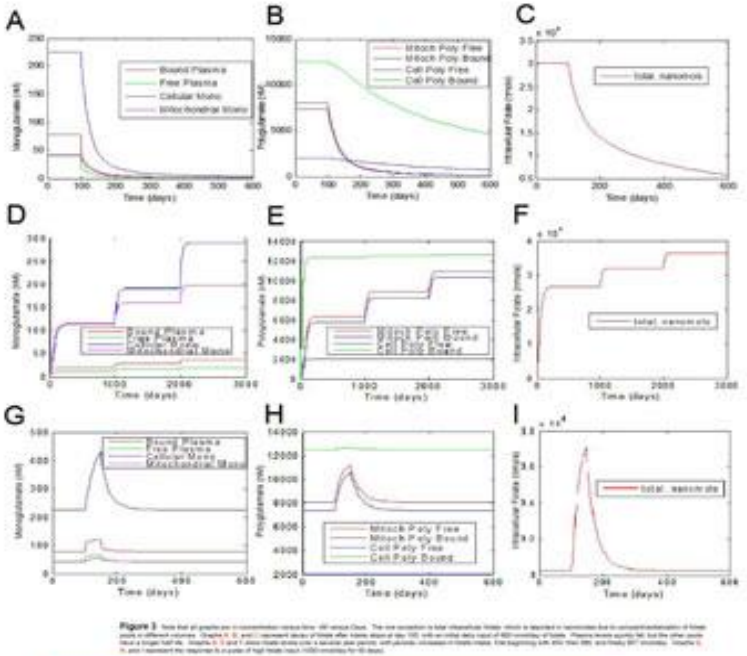

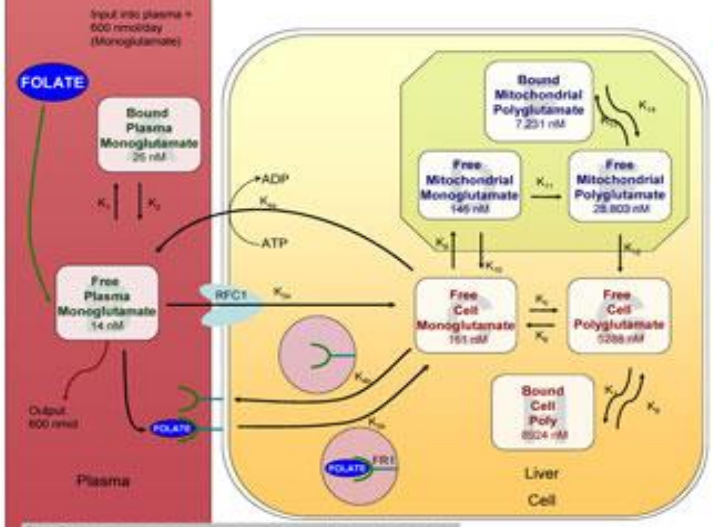

Methods:

Various pool values for plasma and intracellular folate were collected from experimental data (Figure 2). We made predictions for pool values that are not readily available. These predictions were based on known distribution of the various folate pools within the body. For example, 50% of body folate is stored in the liver – the liver contains 2 compartments. These are the cytosol and the mitochondria, each containing three general pools, monoglutamate, free polyglutamate, and bound polyglutamate. These individual pools have different proportions in the cytosol and the mitochondria.

After pool values were established, we assumed that transport of molecules between pools were based on first-order mass-action kinetics. We used Michaelis-Menten equations for the bound polyglutamate pools, because there is a limited amount of protein that will bind to folate – mainly glycine N-methyltransferase (GNMT), one of the enzymes in the methionine cycle (Fig. 1). In addition, we used Michaelis-Menten kinetics for the transport of folates in and out of the cell via Reduced Folate Carrier 1 (RFC1), Folate Receptor 1 (FR1), and an ATP-dependent exporter (Fig. 2).

Rate constants, or k-values, were calculated by assuming certain fluxes between pools. These fluxes were determined by known rates of gain and loss of folate in different compartments where these rates were known, and by adjusting the relative rates of input and output to obtain the right pool sizes between compartments in cases where the absolute rates were not known.

Experiments were performed by varying folate input. These were performed to determine half-lives of the pools, as well as to determine how the pools reacted to example experimental conditions from the literature.

Results:

1. The Model

The model correctly simulates the sizes of the folate pools in the various compartments, including the cytosol, the mitochondria and the fractions bound to proteins in those compartments.

2. Predicted half-life of folate.

After we removed the constant input of folate into the system, all pools diminished over time, some more quickly than others (Figures 3A, 3B). We can also see in figure 3C that the approximate half-life for total intracellular folate is 80 days, which is close to predicted values of around 80-100. Bound polyglutamate seems to decrease at a much slower rate than the other pools.

3. Reaching steady-state values.

The time for the total intracellular pools to reach steady-state typically ranged from 300 to 500 days, which corresponds well with data from the literature. Consistent with the idea that there is a correlation between intracellular folate pool size, polyglutamation, and protein binding, all types of polyglutamate pools do in fact take longer to reach a steady-state value (Figures 3D, 3E).

4. Response to pulsed folate input.

The input of folate was increased to 1000 nmol/day for 50 days. Model plasma levels were quick to rise and fall with the sudden changes, which predicts that free as well as loosely bound monoglutamates will react quickly to changes in folate intake (Fig. 3G). Out of the polyglutamate pools, the model predicts that both bound pools will take longer to return to steady-state, although the mitochondrial bound polyglutamate will take the longest of all of the pools (Fig. 3H).

Conclusions:

We have constructed a mathematical compartment model for folate that takes into account the different methods of transport, as well as retention in the plasma, cell, and mitochondria. We have compared the output of this model with results from current experiments, and have found that the model accurately simulates data from the literature. This model will for the foundation for future studies on the metabolism, transport and sequestration of folates under various genetic and environmental conditions.

Many thanks to Dr. H.F. Nijhout for his guidance and his patience, as well to both Dr. Nijhout and Dr. M.C. Reed for the use of their folate and methionine cycle programs and diagrams. Initial research was supported (in part) by a Howard Hughes Summer Research Fellowship.

Neural Mechanisms Supporting the Cognitive Control of Emotional Information in Schizophrenia

Laura M. Tully, Sarah Hope Lincoln, Todd Wright, Christine I. Hooker
Harvard University

SNAP Lab
Social Neuroscience & Psychopathology

Introduction

- Social impairments are characteristic of schizophrenia(SZ), yet the neural mechanisms that contribute to these impairments remain unknown.
- Successful social interactions require the ability to attend to relevant emotional information and inhibit the irrelevant.
- Studies in healthy individuals indicate that this cognitive control of emotional information requires an intact lateral prefrontal cortex (LPFC).
- Although LPFC deficits are well documented in SZ, it is unclear how these deficits impact cognitive control of emotional information.

We hypothesize:
1) There is dysfunctional activity in the LPFC during cognitive control of emotional information in SZ
2) LPFC activity during emotion control predicts social impairment.

Assessing Cognitive Control of Emotional information

Participants completed 2 cognitive control tasks whilst undergoing fMRI: the Multi-Source Interference Task (MSIT) & our newly created task, the MSIT-Emotion

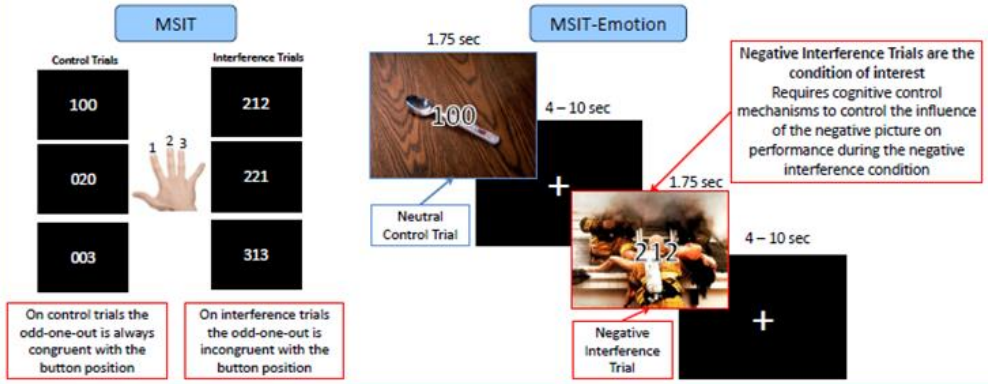

fMRI Results

MSIT
There were no group differences in brain activation on the MSIT

Is there dysfunctional activity during cognitive control of emotional information in SZ?
HCs show greater activation in the DLPFC (BA9) during negative interference trials compared to SZ participants

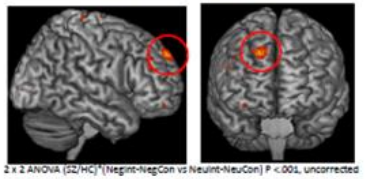

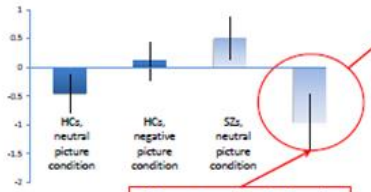

Does DLPFC activity during emotion control predict social impairment?
Although there was not a significant correlation between DLPFC and social impairment, there is a trend in the predicted direction in SZ group.

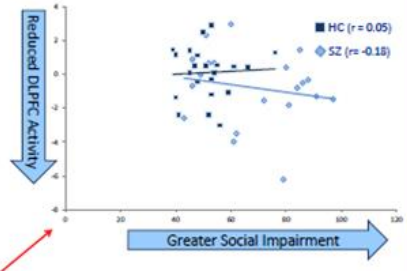

It's possible that the our second hypothesis was not supported due to the contrast between the specificity of our measure of cognitive control of emotion and the broad assessment of social impairments.

Behavioral Data

No group differences on any demographic variables, except social impairments (assessed using SAS-SR)

	HC	SZ
N	22	22
Gender	9F/13M	8F/14M
Age	43.56 (9.42)	41.33 (10.17)
Education	15.33 (3.20)	13.75 (2.60)
IQ	109.13 (14.23)	102.92 (17.56)
Social Impairment	52.11(11.79)	74.02(17.37)**

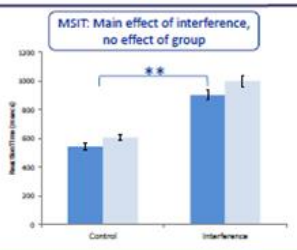

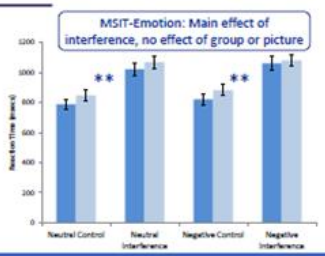

Conclusions & Future Directions

- Results indicate no group differences on a non-affective cognitive control task, the MSIT. However, compared to healthy controls, individuals with schizophrenia have reduced activity in the LPFC during negative interference trials of the MSIT-Emotion.
- However; there was no significant relationship between LPFC activity during negative emotion control and social impairments in the schizophrenia group, thus our second hypothesis was not supported.
- These findings suggest that individuals with schizophrenia have normal LPFC activity during non-affective cognitive control, but fail to effectively engage the LPFC to inhibit irrelevant emotional information. Future analyses will examine the relationship between alternate measure of social impairment and LPFC activity during emotion control.

Necrotising fasciitis due to *Mycobacterium kansasii* in a patient with rheumatoid arthritis on infliximab

Roger P. Clark, DO[1]; Eric T. Tolo, MD[2]; Gerald S. Harris, MD[2]; Sarah K. Zimmerman, MEd[2]; Daniel P. McQuillen, MD[2]

[1]Tufts University School of Medicine, Boston, MA; [2]Lahey Clinic, Burlington, MA

Abstract

A 49-year-old man with rheumatoid arthritis (RA) and gout treated for 4 years with infliximab, methotrexate and prednisone (5 mg daily) presented with a painful, swollen left arm. He had a staphylococcal right elbow ulcer after a gout flare and trauma one year earlier. The ulcer recurred and persisted despite antibiotics and intralesional steroids, biopsy was negative for bacteria. Three weeks prior to presentation nonpainful edema with two large distinct, deeply erythematous plaques developed on his left forearm with peripheral satellite papules. Right elbow biopsy taken 3 weeks earlier showed numerous elongated, beaded mycobacteria. Left arm tenderness ensued. On presentation there was fever to 102.5°F, substantial left extensor forearm fluctuance, and a swollen, tender right index finger PIP joint. No cardiac murmurs were present. No history of travel, swimming or aquarium exposure. WBC was 6000/mm^3 and ESR 13. Left forearm aspirate yielded 57,300 WBC with 80 PMNs and 4+ AFB on smear. Extensive purulence and necrotising fasciitis were found at surgery, requiring debridement of left extensor and flexor forearm fascia and nonviable muscle. All intraoperative specimens grew *Mycobacterium kansasii* with rifampin MIC 0.12 µg/ml; bacterial and fungal cultures were negative. Blood cultures and echocardiogram were negative. Two weeks later debridement of the right index finger also grew *M. kansasii*. Treatment with rifampin, ethambutol, and isoniazid and VAC dressings followed by skin grafts resolved the infection. Methotrexate 7.5 mg weekly and prednisone 6 mg daily without infliximab were resumed 6 months after presentation. Approximately 40 cases of musculoskeletal infection with *M. kansasii*, mostly septic arthritis in compromised hosts or rheumatologic disease, have been described. This is the first reported case of necrotizing fasciitis due to *M. kansasii* and is notable for its subacute presentation and association with infliximab therapy.

Introduction

Mycobacterium kansasii is classified as a slow growing mycobacterium that most often causes pulmonary disease that clinically resembles tuberculosis. It is generally considered to be minimally contagious although it is abundant in the environment. In the United States *M. kansasii* disease occurs most commonly in the Midwestern and Gulf Coast states yielding rare case reports of extrapulmonary disease. The most common extrapulmonary disease is septic arthritis, generally affecting the upper extremities. *M. kansasii* musculoskeletal disease appears to be associated with intraarticular steroids as well as conditions and medications that may lead to an immunocompromised state.

Clinical Course

This case involves a 49-year-old man with rheumatoid arthritis, systemically treated for 4 years with infliximab (injections every 5 weeks), methotrexate (7.5 mg weekly) and prednisone (5 mg daily) who developed a relatively indolent left upper extremity soft tissue infection. This was preceded one year earlier by a traumatic staphylococcal right elbow ulcer approximately that healed but later became chronic despite antibiotics and intralesional steroids. Biopsy was negative for bacteria. Three weeks prior to presentation nonpainful edema with two large distinct, deeply erythematous plaques developed on his left forearm with peripheral satellite papules. Right elbow biopsy taken three weeks earlier showed numerous elongated, beaded mycobacteria. Left arm tenderness ensued.

On presentation there was fever to 102.5°F, substantial left extensor forearm fluctuance, and a swollen, tender right index finger PIP joint. No cardiac murmurs were present. No history of travel, swimming or aquarium exposure. WBC was 6000/mm^3 and ESR 13. Left forearm aspirate yielded 57,300 WBC with 80 PMNs and 4+ AFB on smear. Due to the severity of the appearance and the progressive nature of the process, he was taken to the operating room. Extensive purulence and necrotising fasciitis were found at surgery, requiring debridement of left extensor and flexor forearm fascia and nonviable muscle. All operative specimens grew *M. kansasii* with rifampin MIC 0.12 µg/ml; bacterial and fungal cultures were negative. Blood cultures and echocardiogram were also negative. Two weeks later debridement of the right index finger yielded tissue that also grew *M. kansasii*.

Surgical Findings

Microbiology Methods and Results

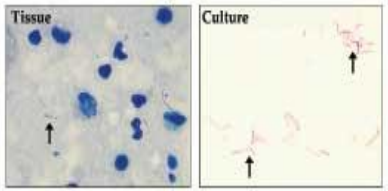

Photochromogen: light exposure → yellow pigment

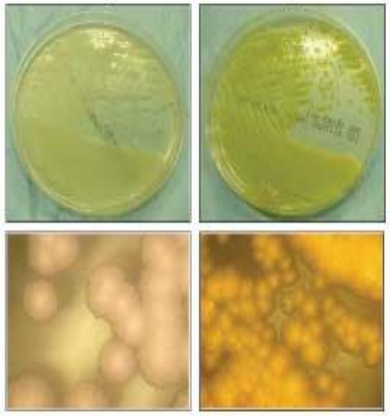

Microbiology Timeline

Day 1: Tissue received. 4+ AFB were seen on direct Kinyoun Stain (Becton, Dickinson and Co., Sparks, MD). Plated directly to liquid and solid mycobacteriological media at room temperature and 37°C.

Day 4: Liquid Mycobacteria Growth Indicator Tube (MGIT) (Becton, Dickinson) at 37°C was positive for acid-fast bacilli. MGIT subbed to selective mycobacteriological media, Mitchinson 7H11 agar (Becton Dickinson).

Day 11: Original solid media positive for a rough, buff colony. Kinyoun stain positive. Culture yielded an atypical mycobacterium whose microscopic characteristics at 1000x were large-sized acid-fast rods with a cross-banding appearance (arrows). Identification as *M. kansasii* made by microscopic and macroscopic morphology, growth rate, pigment production and DNA sequencing. The isolate was rifampin sensitive (MIC 0.12 µg/ml; ARUP, Salt Lake City, UT).

Summary

Mycobacterium kansasii is an acid fast organism that generally causes pulmonary disease and is antigenically similar to *M. tuberculosis*. While an uncommon cause of extrapulmonary infections in humans, the most common manifestations of *M. kansasii* are arthritis and tenosynovitis. There are several risk factors associated with articular *M. kansasii* infections including immunosuppresive medications, rheumatologic conditions such as systemic lupus erythematosis (SLE) or rheumatoid arthritis (RA), psoriasis, AIDS, diabetes mellitus and intraarticular corticosteroids. (1,2)

M. kansasii is environmentally contracted, with the most likely source being tap water, where it has been found to survive for up to a year. (3) This organism is one of the so-called slow growing mycobacteria, and is characterized by being a photochromagen – that is it acquires a yellow pigmentation upon exposure to light. In fact, this bacterium was initially known as the "yellow bacillus" due to this phenomenon.

M. kansasii musculoskeletal infection generally follows a very indolent course, with a mean time to diagnosis of 14 - 17 months. Laboratory studies such as elevated leukocyte count and ESR are not helpful and PPD is often negative. (1,2) While rare, septic arthritis and tenosynovitis are the most common extrapulmonary infections caused by this organism. A literature search did not reveal any cases of necrotizing fasciitis caused by *M. kansasii*. Other atypical mycobacteria that have been reported to cause necrotizing soft tissue infections include *M. ulcerans*, *M. marinum*, and *M. haemophilum*. *M. ulcerans* (Buruli ulcer) is the most commonly reported, with rapid growth of cases in Africa, Australia, India, South America and other tropical regions. Buruli ulcer is characterized by large, well circumscribed necrotic areas of the deep dermis and panniculus.

This patient had multiple predisposing risk factors for mycobacterial infection including RA, gout, intralesional steroid injections, methotrexate, low dose prednisone and infliximab, a systemic tumor necrosis factor inhibitor. After surgical debridement and vacuum-assisted closure accompanied by 12 months of treatment with isoniazid, ethambutol, and rifampin his wounds are well healed with no signs of recurrent infection. Reasonable control of his arthritis was achieved with low dose prednisone and methotrexate resumed 6 months after surgery. Infliximab has not been restarted. This is the first reported case of necrotizing fasciitis due to *M. kansasii* and is notable for its subacute presentation and association with infliximab therapy.

Medial forearm after treatment

Literature Cited

1. Bernard L, Vincent V, Lortholary O *et al. Mycobacterium kansasii* septic arthritis: French retrospective study of 5 years and review. *Clin Infect Dis* 1999;29:1458-60.
2. Nakamura T, Yamamura Y, Tsuruta T *et al. Mycobacterium kansasii* arthritis of the foot in a patient with systemic lupus erythematosus." *Intern Med* 2001;40:1048-9.
3. Joynson, DH. Water: the natural habitat of *Mycobacterium kansasii*? *Tubercle* 1979;60:77-81.

Multidimensional NMR Spectroscopy of Proteins in Living Cells

Leonard D. Spicer,[1] Patrick Reardon,[2] Anne Marie Augustus[2]

[1] Department of Biochemistry and Department of Radiology

[2] Department of Biochemistry
Duke University Medical Center
Department of Biochemistry
Box 3711 DUMC
Durham, NC 27710

Abstract

We have successfully implemented a suite of 3D NMR spectroscopy experiments which provide sufficient data to assign the full backbone resonances of the protein GB1 in live E.coli cells. This represents a unique demonstration that proteins can be studied with detailed NMR characterization in a living cell where the crowded and complex environment likely influences their behavior. The purified and homogeneous samples of proteins and other macromolecules normally studied in structural biology may not reveal this functionally important information. Experiments of this type are essential for de novo assignment of proteins undergoing structural changes in response to perturbing influences such as intermolecular interactions. In-cell multidimensional NMR experiments depend critically on both recent advances in NMR probe performance at high magnetic fields and NMR techniques which considerably reduce the time needed for data acquisition. For the protein GB1, the data were collected using fast projection reconstruction (PR) NMR methods and cryogenically cooled probes on the 600 MHz and 800 MHz NMR spectrometers in the Duke NMR Spectroscopy Center. We have also studied the behavior of the methionine repressor protein, MetJ, using this strategy. Our data suggest that MetJ is primarily associated nonspecifically with DNA in intact cells. This indicates that the repressor likely undergoes linear diffusion along DNA in finding its specific methox recognition sequences rather than the slower random 3D diffusion associated with free cytoplasmic proteins. Support for the NMR Center and the instrumentation used in this research was provided by grants from the NIH and NSF.

Sample Preparation

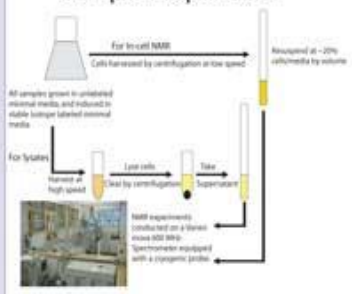

Model Systems

GB1
GB1 is the 56 residue IgG binding domain from Streptococus protein G.

MetJ (shown on DNA)
MetJ is a 24 kDa dimeric repressor protein that regulates the methionine biosynthesis pathway in E.coli.

HCA II
Human Carbonic Anhydrase II is a 29 kDa monomeric enzyme that catalyzes the formation of bicarbonate.

Projection Reconstruction

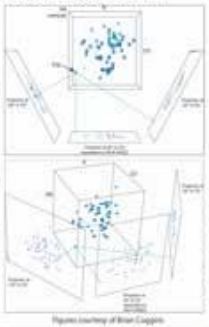

PR-NMR is a reduced dimensionality technique in which data are normally collected in the appropriate orthogonal planes as well as in a series of radially projected planes through the multi-dimensional space.
A projection reconstruction method is then used to combine the 2D data sets into a higher dimensional construct which produces a true multi-dimensional spectrum as illustrated. Since the data are collected in only two dimensions, considerable time is saved in the experiment.

Figures courtesy of Brian Coggins

Cell Viability

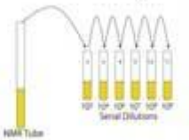

Viability studies were conducted using a microdrop plating assay. 10 µL aliquots were taken from the NMR tube at various time points, and serially-diluted. 10 µL drops are placed on an ampicillin LB agar plate incubated overnight, and colony-forming units counted.

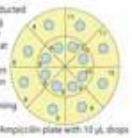

Ampicillin plate with 10 µL drops

GB1

Assignment Spectra

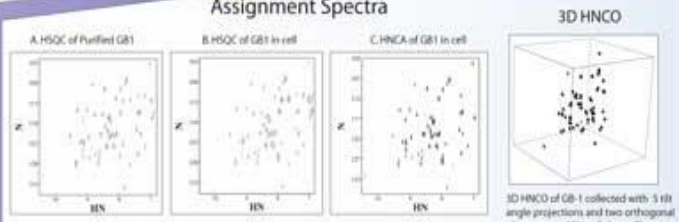

2D plots from (A.) purified GB1, (B.) GB1 in cell, and(C.) a 3D HNCA spectrum of GB-1in cell projected along Ca axis onto HN,N plane. HSQC experiments were collected in ~7 minutes. HNCA was collected in ~2 hrs. In cell spectra were acquired on a ~20% cell slurry. Axis units are ppm.

3D HNCO of GB-1 collected with 5 tilt angle projections and two orthogonal planes on a ~20% cell slurry. The experiment was completed in ~1hr.

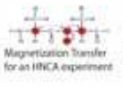

Magnetization Transfer for an HNCA experiment

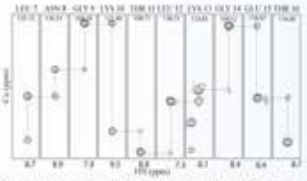

HNCA strip plot showing scalar couplings between HN and Ca carbons in the i and i-1 positions for residues 7-16. The y-axis is ^{13}C chemical shift. The ^{15}N chemical shift for each plane is noted at the top of the strip. In addition an HA(CA)NH data set was also required to complete the assignment. The HA(CA)NH experiment took ~ 3hrs to acquire.

Cell Viability

Cells expressing GB1 remain viable in the NMR tube during the course of our experiments. The first three hours of the data are the average of 2 experiments, while the later time points result from one experiment. Standard deviations are shown for the first three hours.

MetJ

The characteristic HSQC spectrum for MetJ was not visible in whole or lysed cells over expressing MetJ. A. Therefore, pure 15N-labeled MetJ was used in order to ensure there was enough well-folded, well-behaved material for NMR analysis, as well as to eliminate the non-specific background labeling in the cells.
B. When pure 15N labeled MetJ was added to an unlabeled cell lysate, the spectrum completely changed, and the MetJ fingerprint was lost.
C. The fact that MetJ could be re-purified from this lysate, however, shows that MetJ was not being degraded. Instead, binding to or intermediate exchange with components in the lysate (likely DNA) prevent detection of the MetJ signal.

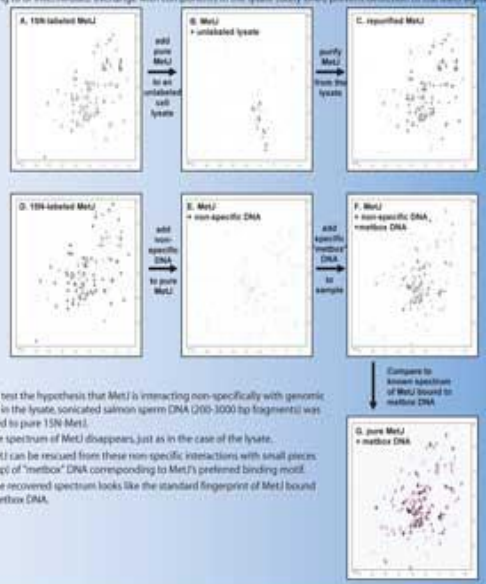

D. To test the hypothesis that MetJ is interacting non-specifically with genomic DNA in the lysate, sonicated salmon sperm DNA (200-3000 bp fragments) was added to pure 15N-MetJ.
E. The spectrum of MetJ disappears, just as in the case of the lysate.
F. MetJ can be rescued from these non-specific interactions with small pieces (20 bp) of "methox" DNA corresponding to MetJ's preferred binding motif.
G. The recovered spectrum looks like the standard fingerprint of MetJ bound to methox DNA.

Human Carbonic Anhydrase II

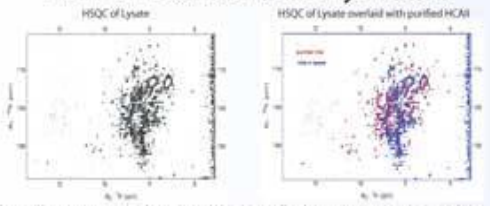

Some HCA II resonances can be observed in a whole cell lysate. The above spectra were acquired on a whole cell lysate of a 500 ml culture. The aquisition time was ~ 2 hours.

Human Carbonic Anhydrase II is generally considered a cytoplasmic enzyme. However, earlier biochemical data have indicated that HCA II may be membrane associated. Association with the membrane could render the protein undetectable by in-cell NMR, due to the increase in rotational correlation time or intermediate exchange. The weak signals detected in this experiment suggest that this carbonic anhydraise isoform maintains some level of membrane association.

Summary

In summary, we have demonstrated the de novo assignment of the small protein GB1 from 3D data collected on whole, living E.coli cells. This was enabled by new NMR experiments incorporating fast projection reconstruction data acquisition and the enhanced sensitivity of cryogenic probes. The implementation of heteronuclear 3D data aquistion in living cells opens a route to previously inaccessible studies of proteins in the biological milieu inside the cell. Furthermore, we have demonstrated how in-cell NMR can yield new insights into the behavior of proteins in their natural environment. In the case of MetJ, the protein may be associated with DNA non-specifically, allowing it to undergo linear diffusion to locate its specific cognate binding site. For HCA II, our data support biochemical results that suggest association with membranes and/or membrane-bound proteins.

References

1. Serber, Z., Dötsch, V. (2001) *Biochemistry* 40, 14317-14323.
2. Serber, Z., Corsini, L., Durst, F. & Dötsch, V. (2005) *Methods Enzymol* 394, 17-41.
3. Wieruszeski, J.-M., Bohin, A., Bohin, J.-P., Lippens, G. (2001) *J Magn Reson* 151, 118-123.
4. Hubbard, S.A., MacLachlan L.K., King G.W., Jones J.J., Foxberry A.P. (2003) *Mol Microbiol* 49, 1191-1200.
5. Dedmon, M. M., Patel, C. N., Young, G. B. & Pielak, G. J. (2002) *Proc Natl Acad Sci U S A* 99, 12681-4.
6. Freeman, R. & Kupce, E. (2004) *Concepts Magn Reson* 23A, 63-75.
7. Kupce, E. & Freeman, R. (2003) *J Biomol NMR* 27, 383-7.
8. Szyperski, T., Wider, G., Bushweller, J. H. & Wüthrich, K. (1993) *J Am Chem Soc* 115, 9307-9308.
9. Kim, S. & Szyperski, T. (2003) *J Am Chem Soc* 125, 1385-1393.
10. Coggins, B. E., Venters, R. A. & Zhou, P. (2004) *J Am Chem Soc* 126, 1000-1.
11. Parkes, J. L. & Coleman, P. S. (1989) *Arch Biochem Biophys* 275, 459-68.
12. Lieberman, D. M. & Reithmeier, R. A. (1988) *J Biol Chem* 263, 10022-8.

SoDA: Somatic Diversification Analysis of antigen receptor recombinations

Joseph M Volpe, Lindsay G Cowell, and Thomas B Kepler

DUKE UNIVERSITY CENTER FOR COMPUTATIONAL IMMUNOLOGY

1 Introduction

The defining characteristic of adaptive immunity is the somatic diversification of its antigen receptor genes. The genes for the T-cell receptor (TCR) and immunoglobulin (Ig) are formed by a process known as V(D)J recombination, in which transcribable genes are composed by the combinatorial joining of gene segments from two or three classes, depending on the specific locus involved. Detailed knowledge of how specific broadly neutralizing HIV antibodies are formed or of the differences in composition between self and non-self antigen receptors is elusive but important for research in vaccine design and autoimmune disorders. Understanding the details of the composition of specific Ig and TCR and the specific processes they underwent during development can facilitate these research endeavors. Thus, we have developed a web-based software tool that analyzes antigen receptor sequences to identify the V, D and J gene segments used, as well as the recombination sites, point mutations and n- and p-nucleotides introduced. We demonstrate the functionality of the software here with an analysis for differential biases within large samples of Ig classified as autoreactive or not.

2 SoDA – (Somatic Diversification Analysis)

SoDA[1] is an implementation of a 3-dimensional algorithm for aligning multiple contiguous DNA sequences to a master antigen receptor sequence in order to determine:

1: the most likely gene segment composition

2: the rules for combining those segments during the formation of an antigen receptor.

Rules for recombination include:

> Identifying recombination sites: some gene segments may undergo exonuclease activity, resulting in a loss of nucelotides in the coding junction.

> Identifying n-nucleotide additions: the enzyme TdT can introduce non-templated nucleotides into the coding junctions.

> Identifying somatic mutations: in B-cells, receptor genes undergo somatic hypermutation, whereby random point mutations are introduced in the gene segments.

3 Why is SoDA unique?

Other bioinformatics solutions already exist (JOINSOLVER[2] and V-QUEST[3]) for approaching this problem, so why build another one? The approach for SoDA is unique in that it relies on dynamic programming, which guarantees an optimal solution. But, unlike typical alignment software, it implements a 3-dimensional algorithm to find it's solution. Formally, SoDA seeks to maximize the likelihood function $P(G,M|T)$, where G = set of gene segments, M=rules for combing those gene segments, T = target sequence, and M(G)=T.

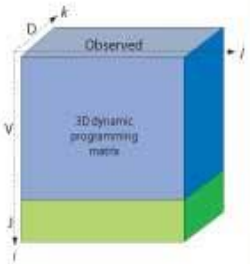

4 3-Dimensional Algorithm

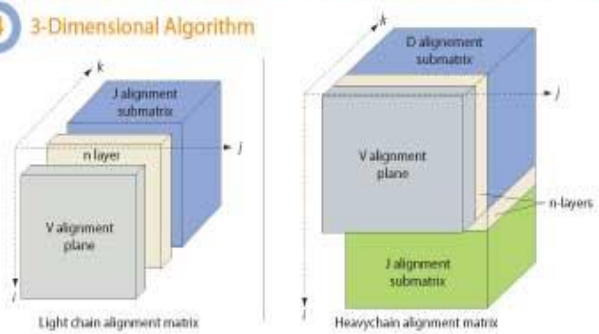

Considering exonuclease activity in the solution adds a constraint to the alignment algorithm: from any point in one gene segment alignment, the traceback path must be able to jump to any point in the contiguous gene segment alignment. For both light and heavy chains, the V alignment is computed in a single plane. Then, the alignment for each contiguous sequence that follows is computed in a 3-dimensional matrix where the alignments run perpendicular to the direction of the alignments for the previous gene segment alignment. This enables the traceback path to jump from any point in one alignment, to any point in the contiguos alignment, thus accounting for the exonuclease constraint. TdT enzymatic activity is captured by the traceback path through the special n-layers.

5 Testing the Algorithm and Results

We tested SoDA using 120 artificial recombination sequences generated by a program that simulates V(D)J recombination. We created 30 sequences at each of four mutation rates: 2.5%, 5%, 10%, and 15%. SoDA proved to be the most reliable in predicting the correct gene segment composition.

	2.5% mutation			5% mutation			10% mutation			15% mutation		
	SoDA	JS	VQ	SoDA	JS	VQ	SoDA	JS	VQ	SoDA	JS	VQ
V correct	30	30	30	30	26	29	30	25	29	30	23	28
D correct	28	26	16	28	28	10	27	25	18	22	19	16
J correct	30	29	29	30	30	28	29	28	29	28	30	30
VDJ correct	28	26	16	28	25	8	27	20	15	22	15	15

SoDA was designed to find the most likely gene segments as well as the most likely rules that created that rearrangment. So, we tested SoDA against 30 rearrangements from Genbank. Below is the CDR3 region of an Ig rearrangement that arguably shows how SoDA's approach finds the best possible explanation for the gene segments and the rules for combining them:

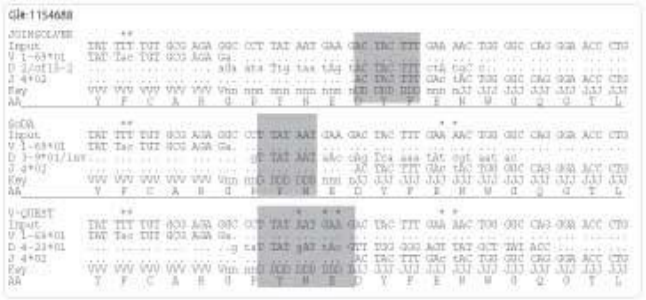

6 Characterizing Autoreactive vs. Non-autoreactive Antibodies

With SoDA, we are able to quatitatively characterize Ig sequences, specifically looking at gene segment usage, CDR3 length, n-nucleotide addition, and mutations. To do this, we downloaded and analyzed approximately 9,450 non-autoreactive Ig and 154 autoreactive Ig sequences from Genbank. Sequences were distinguished and divided into these two groups through keyword searches. Clonal duplicates were removed from each set using an automated procedure that compared several criteria in the sequences.

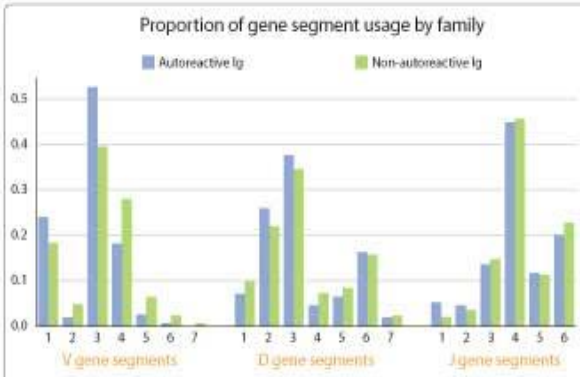

The differences in segment usage between autoreactive and non-autoreactive Ig are contrasted here. The differences in V-gene segment usage are statistically significant.

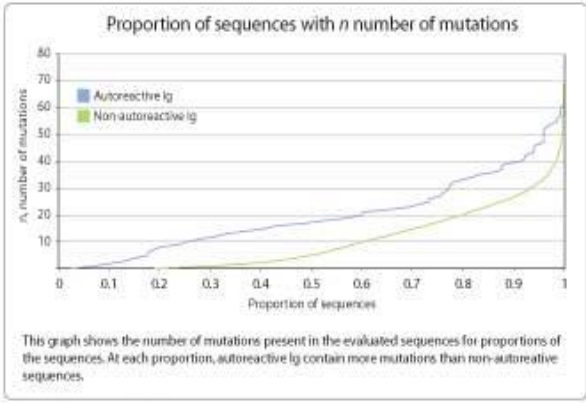

This graph shows the number of mutations present in the evaluated sequences for proportions of the sequences. At each proportion, autoreactive Ig contain more mutations than non-autoreative sequences.

Try out SoDA on the web: **http://dulci.org/soda**

References

1. Volpe, JM. and Cowell, LG, and Kepler, TB. SoDA: implementation of a 3D alignment algorithm for inference of antigen receptor recombinations. Bioinformatics. 2006; 22(4):438-44.

2. Souto-Carneiro, M.M., et al. Characterization of the human Ig heavy chain antigen binding complementarity determining region 3 using a newly developed software algorithm, JOINSOLVER. J. Immunol. . (2004); 172, 6790-6802.

3. Giudicelli, V., et al. IMGT/V-QUEST, an integrated software program for immunoglobulin and T cell receptor V-J and V-D-J rearrangement analysis. Nucleic Acids Res. (2004); 32, W435-W440.

Production de microalgues dans un contexte économique

Niels-Henrik Norsker [a], Maria J. Barbosa [b], Marian H. Vermuë [a], René H. Wijffels [a]

[a] Bioprocess Engineering, Wageningen University, P.O. Box 8129, 6700 EV Wageningen, The Netherlands
[b] Food and Biobased Research, Bornse Weilanden 9, 6708 WG, Wageningen, The Netherlands

WAGENINGEN UR
For quality of life

Introduction

Les microalgues sont des microorganismes qui utilisent la lumière comme source d'énergie pour fixer le dioxyde carbone (CO_2) qui se trouvent en abondance dans les milieux aquatiques (océans, rivières, lacs, etc.).

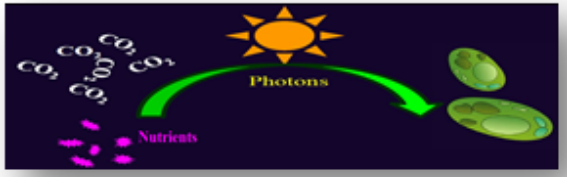

La production de biomasse microalgale à grande échelle représente un véritable défi à la fois biologique, technologique et économique. Durant la dernière décennie, il y a eu le développement de photobioréacteurs à faible coût donnant un meilleur rendement photosynthétique. L'objectif de ce travail est d'évaluer la performance des photobioréacteurs et d'effectuer une optimisation en utilisant les paramètres d'action influençant le rendement photosynthétique ainsi que le coût de la production de biomasse. Dans ce contexte économique, ce travail se propose d'optimiser la culture des microalgues afin d'augmenter la production de biomasse.

Matériel et méthodes

Le coût de la culture de microalgues a été calculé pour 3 systèmes différents exploités aujourd'hui à l'échelle commerciale : les bassins ouverts (A), les photobioréacteurs plans (B) photobioréacteurs tubulaires-horizontaux (C).

Résultats

L'optimisation de la production en utilisant ces facteurs permet de minimiser le coût, ce qui fait des micro-algues une matière première prometteuse pour la production de biodiesel. Le photobioréacteur tubulaire est le plus économique pour la production de biomasse dans des conditions néerlandaises.

Table 1 : Sensitivity analysis. Biomass cost in € per kg with different scenarios (100 ha plant)

Facteurs	Bassins ouverts (€/kg)	Photobioréacteur tubulaire (€/kg)	Photobioréacteurs plans (€/kg)
1. Cas de base	4.95	4.16	5.96
2. Emplacement	2.83	2.44	3. 26
3. Homogénéisation		3. 06	3. 08
4. CO2	4. 61	2. 72	2. 74
5. Milieu	4.17	2. 28	2. 30
6. Photosynthèse	2. 61	1. 43	1. 44
7. Emplacement	1. 28	0. 70	0. 68

Discussion

L'utilisation des microalgues comme source d'énergie permet d'atteindre des rendements surfaciques élevés, une teneur en huile élevée de certaines souches, une faible consommation d'eau et la possibilité de production dans des zones arides (1,2). Les systèmes ouverts souffrent de productivité de la biomasse basse et des coûts élevés de récolte de la biomasse en raison des faibles densités de biomasse, l'utilisation de grandes surfaces, les pertes de carbone dioxyde de carbone et de faibles possibilités de contrôle des contaminants (3).
Les microalgues peuvent conserver un maximum de 9-10% de l'énergie solaire (rendement photosynthétique), mais les systèmes de production de microalgues en plein air dépassent rarement les 6%. Cependant, de nouvelles méthodes de modifications génétiques ont été développées pour améliorer l'efficacité photosynthétique (4).
Durant la dernière décennie, il y a eu le développement de photobioréacteurs à faible coût qui appliquent le principe de la lumière diluée donnant un meilleur rendement photosynthétique (5).
Les bassins ouverts sont peu profonds et la densité de biomasse est faible (0.3 g en poids sec par litre). Le processus nécessite beaucoup moins d'énergie pour l'homogénéisation que les deux autres conceptions de réacteurs, mais en raison de la faible densité de biomasse est, le coût nécessaire à la récolte est un facteur limitant. Ce type de réacteur est largement utilisé dans la production industrielle de microalgues, par exemple pour produire Spirulina et Dunaliella avec une quantité de 5000 t et 1200 t par an, respectivement (6).

Le principe des photobioréacteurs tubulaires est que la culture de microalgues circule cycliquement par une pompe centrifuge entre un réseau de tubes transparents et une colonne de dégazage. Dans les photobioréacteurs tubulaires, l'agitation est créée par la turbulence. Mais la turbulence est coûteuse à produire en termes d'apport énergétique. Il y a aussi la contrainte des forces de cisaillement. L'oxygène tend à s'accumuler à des concentrations qui inhibent la photosynthèse, ce qui diminue la productivité algale. Il est donc important d'optimiser le dégazage. Les parois transparentes sont classiquement constituées de plastique ou de verre avec une durée de vie d'un an. L'agitation est un paramètre critique pour mélanger les cellules entre les zones éclairées à la périphérie du tube et les zones sombres autour du centre. Avec ce système, une densité de biomasse de 1,7 g en poids sec par litre est obtenue. Les photobioréacteurs tubulaires sont utilisés en industrie par exemple pour la production d'un pigment par l'algue Haematococcus et aussi pour ma production Chlorella et Nannochloropsis.
Les photobioréacteurs plans sont transparents pour faire laisser passer la lumirère. L'agitation se fait par l'air avec un niveau d'aération de 1 litre du volume du bioréacteur par minute (7). La concentration de biomasse est de 2.1 g en poids sec par litre. Un tel système a été démontrée efficace, par exemple pour la production de souches d'algues qui accumulent des lipides sous limitation en nutriments. Pour les photobioréacteurs plans, le coût est fortement affecté par le flux d'air, le coût d'alimentation et du ventilateur. Il est possible qu'une meilleure économie puisse être obtenue avec d'autres types de ventilateurs (8).

Conclusion

Il est très important de sélectionner un système approprié pour cultiver les microalgues avec un rendement élevé. Actuellement, les systèmes proposés sont les bassins ouverts et les photobioréacteurs ; chacun avec des avantages et des contraintes avec variation de la productivité pour chaque système de production.
Un photobioréacteur plus économique permettant une culture maîtrisée (température, radiation, pH, nutriments…) et en continu des microalgues facilitera des approches nouvelles de recherches dont les résultats pourront être mis en application.
Cette approche économique permet également de souligner les efforts à fournir dans les différents systèmes pour assurer une meilleure production de microalgues à l'échelle industrielle.

Références

1. BP. BP and Martek biosciences enter a joint development agreement to deliver advanced biodiesels. Retrieved 09.05.10; 2009.
2. Mascarelli AL. Gold rush for algae. Nature 2009;461(7263):460–1.
3. Posten C. Design principles of photo-bioreactors for cultivation of microalgae. Eng Life Sci 2009;9(3):165–77.
4. Carvalho AP, Meireles LA, Malcata X. Microalgal reactors: a review of enclosed system designs and performances. Biotechnol Prog 2006;22(6):1490–506.
5. Pulz O, Scheibenbogen K. In: Scheper T, editor. Photobioreactors: design and performance with respect to light energy input. Springer : Berlin Heidelberg; 1998. p. 123–52.
6. Spolaore P, Joannis-C C, Duran E, Isambert A. Review: commercial applications of microalgae. J Biosci Bioeng 2006;101(2):9.
7. Sierra E, Acién FG, Fernández JM, García JL, González C,Molina E. Characterization of a flat plate photobioreactor for the production of microalgae. Chem Eng J 2008;138(1–3):136–47.
8. Rodolfi L, Zittelli GC, Bassi N, Padovani G, Biondi N, Bonini G, et al. Microalgae for oil: strain selection, induction of lipid synthesis and outdoor mass cultivation in a lowcost photobioreactor. Biotechnol Bioeng 2009;102(1):100–12.

Faisabilité de la paille de riz comme substrat alternatif pour produire du biobutanol

Amrita Ranjan, Swati Khanna, V.S. Moholkar
Centre info-énergie, Indian Institute of Technology Guwahati, Guwahati 781 039, Assam, Inde

Introduction

En raison des fluctuations récentes du prix du pétrole brut et les préoccupations croissantes sur l'environnement, de plus en plus d'attention a été consacrée au développement des ressources d'énergies alternatives rentables et respectueuses de l'environnement [1]. Le biobutanol est un carburant alternatif idéal en raison de sa haute teneur en énergie. Dans le scénario indien, la paille de riz est l'une des matières premières lignocellulosiques les plus abondantes, [2], contient un mélange de sucres choisis pour la production de biobutanol par fermentation ABE [3]. La paille de riz prétraité acidifié a été utilisé comme substrat pour la production de biobutanol par *Clostridium acetobutylicum NCIM 2337.*

Objectif

- Utilisation de la paille de riz pour la production de biocarburant alcoolique.
- La production de l'ABE par fermentation clostridiale RSH

Materiels et methodes

1. Maintien de la culture et de la croissance

Spores séchées de *C. acetobutylicum NCIM 2337* ont été ravivées par voie anaérobie en RCA et les médias de la MRC de la culture (Bouillon) à inoculé dans un erlenmeyer de 250 ml

2. Inoculum

Les cultures de *Clostridium* ont été incubées en anaérobiose sur RCA jusqu'à ce que la croissance active a été observée. Seule colonie de *Clostridium* a été transférée au bouillon MRC, et a été ré-incubée à 37 ° C. 5% des cultures t de *C. acetobutylicum NCIM 2337* ont été ajoutés par la suite à la cuve expérimentale.

3. Hydrolysat de paille de riz

5% p / v du mélange de paille de riz, soit 75 g de paille de riz ajoutés à 1500 ml d'eau acidifiée bidistillée (1% H_2SO_4), a été prise dans un récipient spécialement conçu au prétraitement du volume 2 L. Ce mélange a été agité, autoclavé et on laisse refroidir à température ambiante. La suspension de la paille de riz a été filtrée. Petites aliquotes ont été prises à différents stades du prétraitement.

4. Fermentation

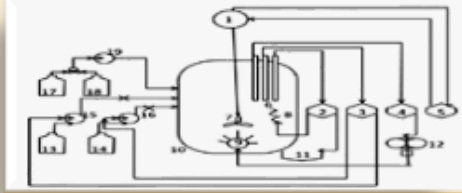

Fig. 1. Organigramme lot réacteur: (1): moteur, (2): affichage de la température à du module de commande, (3): indication du pH et du module de commande, (4): affichage d'oxygène dissous et le module de commande, (5): affichage de la vitesse d'agitation et Module de contrôle, (6): les sondes, (7): un agitateur, (8): chauffage, (9): arroseur, (10): autoclavable récipient en verre de borosilicate, (11): refroidisseur, (12): la pompe à air, (13): réservoir d'acide, (14): réservoir de base, (15): pompe péristaltique pour acide, (16): pompe péristaltique pour la base, (17): les médias réservoir, (18): réservoir de récolte et (19): alimentation / pompe péristaltique récolte.

Analyse

Résultats

1 Pré-traitement de la paille de riz

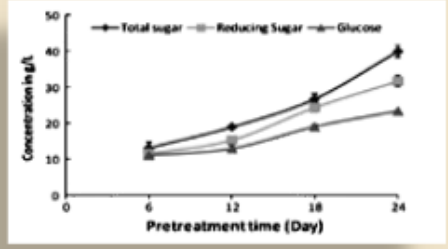

Fig. 2. Publication du sucre pendant le prétraitement de la paille de riz

2 La croissance de *C. acetobutylicum NCIM 2337*

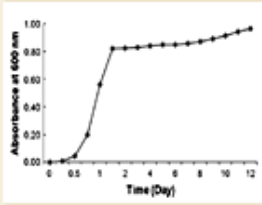

Fig. 3. Courbe de croissance de *C acetobutylicum NCIM 2337* lors de la fermentation, en utilisant hydrolysat de paille de riz comme matière première

3 Utilisation du sucre pendant la fermentation

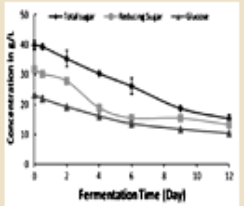

Fig. 4. Utilisation du sucre pendant la fermentation clostridiale de l'hydrolysats de paille de riz

4 Production de solvants lors de la fermentation

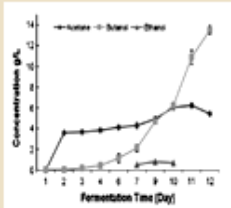

Fig. 5. La production d'acétone, de butanol et d'éthanol pendant la fermentation de l'hydrolysat de paille de riz.

Discussion

- En comparant la composition en sucres pour la fermentation des hydrolysats obtenus en utilisant d'autres matières premières alterne avec des RSH (présent ouvrage); donnera importance relative des RS comme matière première alternative potentielle pour la fermentation ABE [4]. La teneur en glucose de l'hydrolysat avec cette technique est comparable à l'hydrolysat obtenu par Qureshi et al. avec la technique de l'acide assisté traitement enzymatique de fibre de maïs [5] . Ceci démontre l'efficacité de la technique d'hydrolyse acide de cisaillement assistée de RS utilisées dans la présente étude. Il pourrait être perçu que la fermentation d'hydrolysat de paille de riz a entraîné une utilisation incomplète du sucre.
- l'utilisation complète des sucres par la culture microbienne avec une production accrue de solvants. Supplémentation en outre de la paille de riz avec l'extrait de levure et le p-amino benzoïque se traduira par l'utilisation presque complète du sucre avec le profil de solvant élevé.
- Comparaison des résultats de la présente étude utilisant un bioréacteur, avec les études antérieures de niveau flacon révèle l'acétone beaucoup plus élevé et la production de butanol.
- Un rendement total élevé de solvants FBA dans la présente étude peuvent être apportés par fraction plus élevée de glucose dans RSH, comme clostridies préférence à utiliser le glucose.

Conclusion

Ces résultats démontrent clairement candidature de RS en tant que substrat économique de rechange à utiliser en fermentation microbienne. La production des solvants peut être encore améliorée par la supplémentation en nutriments de l'hydrolysat de paille de riz grâce à l'amélioration nutritionnelle, l'utilisation de souches génétiquement modifiées et l'optimisation des paramètres physiques tels que le pH et la température.

Références

[1] Srirangan K, Akawi L, Moo-Young M, Chou CP. Towards sustainable production of clean energy carriers from biomass resources. Appl Energy 2012. doi: 1016/japenergy.2012.05.012.
[2] Gadde B, Menke C, Wassmann R. Rice straw as a renewable energy source in India, Thailand and the Philippines: overall potential and limitations for energy contribution and greenhouse gas mitigation. Biomass Bioenergy 2009;33:1532–46.
[3] He Y, Pang Y, Liu Y, Li X, Wang K. Physicochemical characterization of rice straw pretreated with sodium hydroxide in the solid state for enhancing biogas production. Energy Fuel 2008;22:2775–81.
[4] Weil JR, Dien B, Hendrickson R, Mosier NS, Ladisch MR. Removal of fermentation inhibitors formed during fermentation of biomass by polymeric adsorbent. Ind Eng Chem Res 2002;41:6132–6.
[5] Liu Z, Ying Y, Li F, Ma C, Xu P. Butanol production by Clostridium beijerinckii ATCC 55025 from wheat bran. J Ind Microbiol Biotechnol 2010;37:495–501.

Sidi Ali Imène

Production et l'optimisation de protéase acide par *Aspergillus spp* par fermentation submergée

S. Radha, V. J. Nithya, R. Himakiran Babu, A. Sridevi, NBL Prasad and G. Narasimha*

Département de Biotechnologie , SVEC, A.Rangampet ,Département de Biotechnologie, SPMV , faculté d'ingénierie , Tirupati, Insitut de recherche technologique de pétrole, JNTU, Anantapu , Laboratoire de Microbiologie appliquée, Département de Virologie, Université Sri Venkateswara, Tirupati, A.P, Inde

Introduction

Les protéases sont la classe la plus importante parmis les enzymes industrielles, et représentent environ 25% des enzymes commerciales dans le monde (1) , elles sont classeés en trois classes : des protéases acides , neutres et alkalines (2) .

Les protéases sont essentiellement produites par la fermentation submergée (3) .

La moisissure du genre *Aspergillus* est utilisée pour la production de protéases parceque plusieurs espéces de ce genre ne présentent pas un danger .(4)

La mélasse est une matiére premiére trés intéressente pour la production de protéase par les microorganismes (5) Parcequ'elle est :

- riche en nutriments et en minéraux
- Avec un prix raisonnable
- présente dans plusieurs sous produits d'industrie sucriére

Figure 1 : les Mélasses

Les objectifs

❖Déterminer la potentialité de mélasse comme un substrat principal et leur combinaisons avec le lactosérum .

❖Déterminer les autres conditions optimales de milieu de fermentation pour produire une protéase extracellulaire par *Aspergillus*

Méthodes et Matérielles

▪Les échantillons ont été collectés a partir des sites contaminés par les déchets d'abattoir des zones rurales de Tirupati en Inde.

❖**Isolements et ensemencement de la moisissure :**

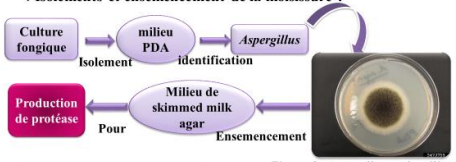

Figure 2: *Aspergillus* sur le milieu de PDA

❖**Préparation d'inoculum:**

❖Fermentation

50 ml de Mélasses stériles + 2ml de suspension de spores fongiques → Agitation ⇨ filtration

Le filtrat est ensuite utilisé pour la production de protéase en modifiant la méthode de Anson (3) .

Table 1: Expériences sur les différentes conditions optimales pour le milieu de fermentation

Paramètres	Expériences
1) Les Mélasses	L'effet de différentes combinaisons de lactosérum avec les mélasses .
2) Température	L'Effet de différentes températures à partir de 25°±2°C et 32°±2°C jusqu'à 55°±2°C.
3) Le temps d'incubation	3 à 7 jours avec un milieu constitué par des volumes égaux de mélasses et de lactosérum avec un pH initiale de 6.2 à une température de 32°C.
4) pH	L'Effet de différentes PH allant de 2 à 9 avec le milieu préparé 1:1
5) Source d'azote	L'Effet de différentes sources d'azote à 1% ont été ajoutés au milieu de mélasses et lactosérum .
6) Source de carbone	L'Effet des différentes sources de carbones
7) Céréales	Milieu enrichi par 1% des différentes Farines de céréales

Résultats

1) l'effet des mélasses et du lactosérum sur la production de protéase :

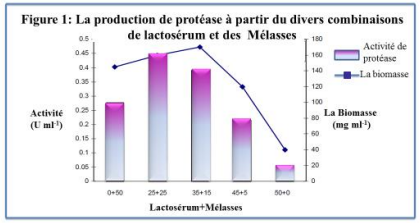

2) Le temps d'incubation

Le meilleur temps d'incubation a été trouvé 120h.

3) l'effet de la température

Table 2 : représente l'effet de différentes températures sur la biomasse et la production de protéase .

Température °C	Activité de protéase	poids sec de Mycélium
25±2°C	0,3350	32,25
32±2°C	0,4481	56,40
55±2°C	0,2315	25,24

4) L'effet de pH :

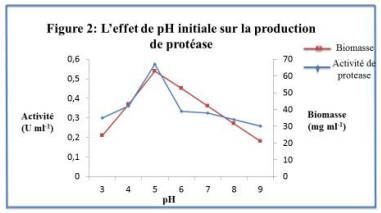

5) L'effet de différentes sources d'azotes :

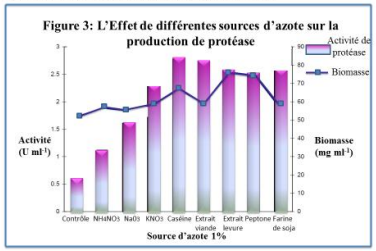

6)L'effet du différentes sources de carbone :

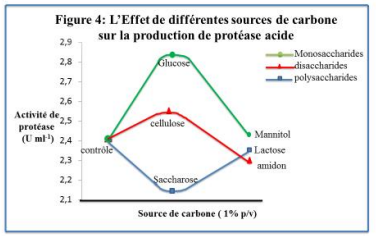

7)Effet de céréales sur la production de protéase :

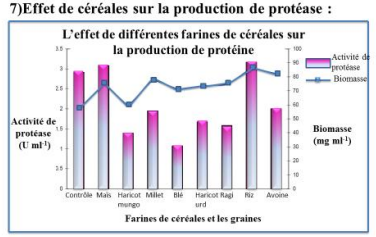

Discussion

1) L'effet de lactoserum avec les mélasses : l'utilisation de lactosérum avec les mélasses a amélioré la production de protéase , parcequ' il réprésente une bonne source d'azote , des observations similaires ont été trouvées par Usama F.Ali.(2008) (6). Et aussi Francisco *et al.* (2008) (7) qui a utilisé le lactosérum pour la production de protéase par *Serratia marcescens.*

2) l'Effet de différentes température : la température optimale a été trouvée 32±2°C ,et l'activité de protéase commence a diminuer à partir de 55°C , cela peut être dû au fait que les températures élevés peuvent dénaturer les enzymes .

3) L'effet de différents PH : la production maximale d'enzyme et du poids sec fongiques ont été observés au pH égale à 5.0. Ganesh Kumar (2008) (8) a indiqué que le pH optimale pour le protéase acide était entre 5.5- 6.5 à partir des déchets solides de tannerie par des espéces synergistes .

4)L'effet de différentes sources d'azote : le milieu supplimenté par une source organique d'azote supporte une production de protéase plus élevé par rapport au source inorganique ,des observations similaires ont été trouvées par Narayana *et al.* (2008)(1).

5)l'Effet de différentes sources de carbone: l'utilisation des monosaccharides a améliorée la production de protéases , des observations similaires ont été touvées par Narayana *et al.* (2008) (1) qu'ils ont indiqués que des sources de carbone tell que le glucose sont des composants indispensables pour la production de protéase .

6)L'effet des différentes farines des céréales : la farine de maïs et la farine de riz ont montrées une augmentation significative dans la production de protéase lorsqu'elles sont comparées avec le contrôle.

Des travaux ont été réalisés en parallèle ont montrés que les concentration optimales pour la production de protéase sont de 4% pour l'inoculum fongique et 1% pour la farine de soja .

Conclusion

En se basant sur les résultats de cette étude on peut conclure que :

- Les mélasses et le lactosérum sont des substrats appropriés pour la production de protéase dans une fermentation submergée par *Aspergillus spp*
- les conditions culturelles ont été optimisées à un pH de 5.0, une température de 32±2°C et un temps d'incubation égale à 120 h.
- Le glucose est la source de carbone la plus efficace .
- 1% de farine de riz a augmenteé la production de protéase .
- La farine de soja est le substrat le moins cher comme source d'azote mais leur production de protéase est moins par 13% de celle de la caséine .

Références

1) K.J.P.Narayana,M.Vijayalakshmi (2008), *Asian Journal of Biochem* . 3, 3, 198-202.
2) C.Djamel T. Ali, C. Nelly,.(2009), *European journal of Scientific Research.* 25, 3, 469-477.
3) S. Sinha .(2009), *International Journal of Food Engineering.*
4) C. Sandhya, A. Sumantha, G. Szakacs, A.(2005) ,Process Biochem . 40, 2689-2694.
5) Magdi A.M.Younis, Francis F. Hezayen *and al* .(2009) ,*Global Journal of Biotech and Biochem* . 4(2): 132-137.
6) Usama F.Ali.(2003), *Research Journal of Agriculture and Biological Sciences* . 4(6): 886- 891.
7) Francisco *et al.*(2008) , Fermentation conditions increasing protease production by *S.marcescens* in fresh whey, *Rev.Tec.Ing.Univ.Zulia*.31,1.
8) A. Ganesh *et al.*(2008), *Bioresource Technol.* , 99, 7,2364-72.

Remerciements

Les auteurs expriment leur gratitude au faculté d'ingénierie de Vidhyanikethan pour la fourniture d'équipement de laboratoire nécéssaire pour la réalisation de cette étude .

Optimisation du prétraitement du sorgho photopériodique sensible pour production d'éthanol

Feng Xu [a] ,Karnnalin Theerarattananoon [a] ,Xiaorong Wu [a], Leidy Pena, Yong-Cheng Shi [b],Scott Staggenborg [c],Donghai Wang[a],*

[a] Département de génie biologique et agricole, [b]Département science des grains et de l'Industrie,[c] Département d'Agronomie, Université Kansas State

Introduction

Le sorgho photopériodique sensible (PS) est une culture caractérisée par sa remarquable résistance à la sécheresse . C'est une biomasse compétitive au blé pour production d'éthanol par sa forte teneur en sucre soluble .

Un prétraitement de la biomasse par l'acide sulfurique est appliqué, pour rendre la cellulose facilement dégradable ,réalisant ainsi une efficacité élevée de l'hydrolyse enzymatique (EEH) en glucose fermentescible(1).

Selon l'étude précédente 74% de la source de sucre est converti en éthanol . la perte de Cellulose (glucose) par dégradation à l'état acide n'est pas négligeable(1) .

Objectif

L'objectif de cette étude est d'optimiser le prétraitement pour maximiser la quantité totale de glucose obtenue qui permet d'atteindre des rendements élevés en éthanol.

Matériels et méthodes

Les étapes du processus de conversion de la matière lignocellulosique en bioéthanol

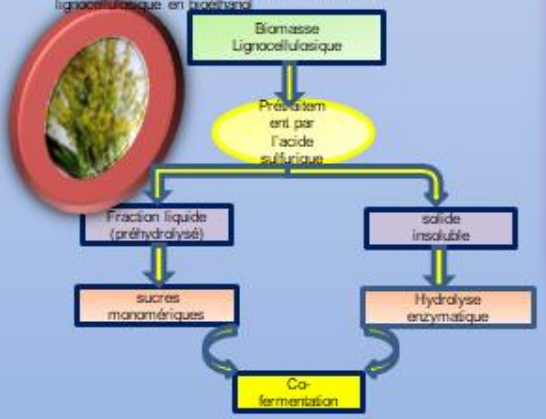

Résultats

Tableau 1:conception expérimentale avec la méthodologie de surface de réponse(RSM)

Ech	Temp	Temps	Concentration	Yrec(%)
1	180	40	0.5	67.77
2	160	50	1.5	84.91
3	160	40	1	89.54
4	180	30	1	91.82
5	180	50	1	89.43
6	160	40	1	89.66
7	160	50	0.5	88.66
8	160	30	1.5	84.84
9	140	40	0.5	94.84
10	140	50	1	94.94
11	180	40	1.5	90.39
12	180	40	1.5	90.39
13	160	40	1	90.11
14	160	30	0.5	95.71
15	140	30	1	94.09

$$Y_{REC} = -1041.8 - 13.65 \times A + 3.893 \times B + 129.8 \times C - 0.02506 \times A \times B - 0.888 \times A \times C - 0.04014 \times A^2$$

Figure1:surface de réponse 3-D de EEH

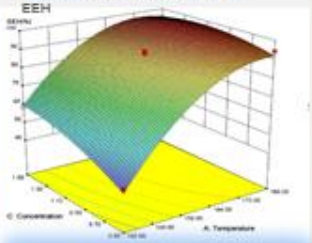

EEH= -1064.5+12.47×A +0.2951×B+103.3×C-0.3908×A×C/0.0435×A²-14.73×C²

Figure2:Surface de réponse 3-D du rendement en glucose totale en fonction du temps et température ; température et concentration

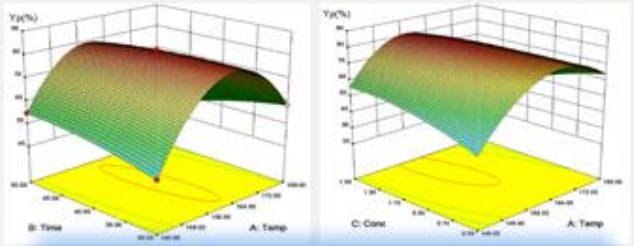

$$Yp = -193.26 - 1424.9 \times C + 0.06042 \times A \times B + 19.58 \times A \times C + 7.855 \times 10^{-3} \times A^2 - 0.02683 \times B^2 - 17.14 \times C^2 - 2.930 \times 10^{-4} \times A^2 \times B - 0.06494 \times A^2 \times C$$

Discussion

Grâce à l'analyse et à l'optimisation par la méthodologie de surfaces de réponse (RSM), trois modèles ont été obtenus EEH, Yrec, et Yp .

Après prétraitement à l'acide sulfurique, l'efficacité de l'hydrolyse enzymatique (EEH) a augmenté contrairement à la diminution du rendement de récupération de la cellulose (Yrec) lors de l'élevation des 3 variables du prétraitement (concentration , température, temps).

Cette augmentation du EEH et diminution du Yrec pourrait résulté du fait que la structure cellulosique a été perturbée (2) ,ce qui a augmentée la surface de la cellulase lors de l'hydrolyse enzymatique(3). La baisse du Yrec peut aussi être expliqué à ce que la plupart des parties amorphes (hémicellulase et lignine) ont été dégradées. (1)

Conclusion

L'optimisation simultanée de l'hydrolyse enzymatique et du rendement de récupération de cellulose du sorgho PS par RSM, en se référant au rendement du glucose total ,a permis d'atteindre un rendement de glucose maximal de 82,8% uniquement de la partie solide prétraitée.

Référence

(1) Xu, F., Shi, Y.-C., Wu, X., Staggenborg, S., Wang, D., 2011.Sulfuric acid pretreatment and enzymatic hydrolysis of photoperiod sensitive sorghum for ethanol production. Bioprocess and Biosyst Eng.34 (4),485–492.

(2) Zeng,M., 2007.Microscopic examination of changes of plant cell structure in corn stover due to hot water pretreatment and enzymatic hydrolysis. Biotechnol.Bioeng.97 (2) 265.

(3)Fan, L., Lee, Y., Beardmore, D., 1980. Mechanism of the enzymatic hydrolysis of cellulose: effects of major structural features of cellulose on enzymatic hydrolysis.Biotechnol.Bioeng.22 (1), 177–199.

Ferroudji Sarra

Ingénierie métabolique de *Pseudomonas fluorescens* productrice de vanilline à partir d'acide férulique

Maurizio Ruzzi [a,*], Diana Di Gioia [c,1], Francesca Luziatelli [a,1], Andrea Negroni [b], Anna Grazia Ficca [a], Fabio Fava [b]

[a] Department pour l'innovation en Biologie, Agroalimentaire et Systèmes forestiers, Université de *Tuscia, Italie*

[b] Department de génie civil, de l'environment et de génie des Materiaux , Université de *Bologne, Italie*

[c] Department des sciences et technologies Agro-environment, Université de *Bologne, Italie*

Introduction

La vanilline est le principal composé de vanille, la saveur la plus importante en industries alimentaires(1). Elle peut être produite par des procédés biotechnologiques à partir de sources naturelles, telles que l'acide férulique (2), en utilisant des micro-organismes, tels que les souches recombinantes *Escherichia. coli* : parmi les productrices les plus efficaces de vanilline (3). *Pseudomonas* sont connus pour leur polyvalence métabolique et leur plasticité génétique et certaines souches, comme *Pseudomonas fluorescens* BF13, dégrade l'acide férulique formant la vanilline comme un intermédiaire catabolique (4).

Objectif

Le but de ce projet était de développer des dérivés de *P. fluorescens* BF13 capables de convertir l'acide férulique en vanilline et d'optimiser certains paramètres qui influent sur leur activité catalytique.

Méthodes

Inactivation du gène codant pour la vanilline déshydrogénase (*vdh*) en utilisant un plasmide suicide (pU-vdh::Km)

Transformation des cellules par électroporation.

La sélection se fait sur un milieu LB contenant le kanamycine, une de ces mutantes désigné BF13-1p4 a été transformé avec le plasmide pBB1 pour restaurer l'activité de gène catabolique de l'acide férulique (*fcs*).

Les expériences de bioconversion ont été réalisées avec des cellules en maintenance cultivées sur LB à 30°C.

L'induction du gène (*fcs*) se fait avec l'acide férulique (2,5 mM) à 1,5 ou 3 h après l'inoculation.

La culture a été effectuée en flacons secoués de 2L, avec 100 mL de milieu de culture, ou en fermenteur de laboratoire de 3L avec 2L de milieu de culture.

La croissance a été suivie en mesurant l'augmentation de l'absorbance (A600) et le poids humide.

Consommation d'acide férulique et la formation de la vanilline sous agitation a été suivie par HPLC-DAD.

Résultats et discussion

Inactivation du gène *vdh*: elle a un fort effet polaire sur l'expression du gène *fcs*. La transformation du BF13-1p4 avec le plasmide pBB1 restore l'activité de

Production de la biomasse:

Fig.1. La biotransformation de l'acide férulique (carré) en vanilline (triangle) et les produits d'oxydation de vanilline (acide vanillique, cercle) par les cellules en maintenance la souche *P. fluorescens* BF13-1p4 (pBB1) exposée à l'acide férulique à 1,5 h (symboles pleins) et 3 h (symboles vides).

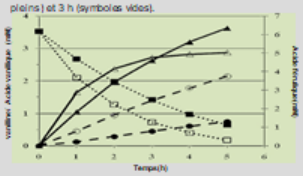

Fig. 2. La courbe de croissance de *P. fluorescens* BF13-1p4 (pBB1) dans un réacteur à cuve agité (3L) surveillé à A600 (symboles pleins) et le poids humide (symboles vides).

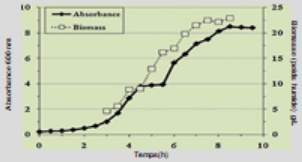

Processus de bioconversion:

Fig. 3. La production de la vanilline (A) et l'acide férulique résiduel (B) en utilisant différentes concentrations de la biomasse dans la gamme de 3-6 g (poids humide)/ L sur une période de 24

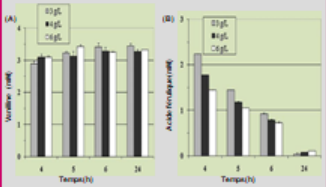

Résultats et discussion

Fig. 6. La biotransformation de l'acide férulique (diamant) en vanilline (carré) et les produits d'oxydation de vanilline (acide vanillique, triangle)

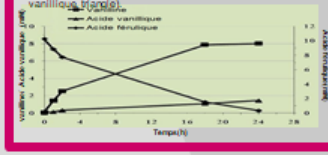

Conclusion

Pseudomonas fluorescens n'est pas une bactérie pathogène utilisée dans de nombreuses applications. L'inactivation du gène (vdh) par insertion et l'amplification du gène (*fcs*) simultanément, nous avons réussi à développer une souche recombinante de *P. fluorescens* capable de convertir l'acide férulique en vanilline. L'optimisation des conditions de culture et de production en petit et grand échelle à la fois pourrait conduire à une amélioration de la productivité de la vanilline jusqu'à 8,41mM.

Références

1. **Walton, N.J., Mayer, M.J., Narbad, A.**(2003) Vanillin. Phytochemistry 63, 505–515.
2. **Havkin-Frenkel, D., Belanger, F.C**(2008) Biotechnological production of vanil. In: in: Havkin-Frenkel, D., Belanger, F.C. (Eds.), Biotechnology in Flavor Production. Wiley-Blackwell, Oxford, UK, pp. 83–103.
3. **Yoon, S.H., Cui, L., Lee, Y.M., Lee, S.H., Kim, S.H., Choi, M.S., Seo, W.T., Yang, J.K., Kim, J.Y., Kim, S.W.**(2005) Production of vanillin from ferulic acid using recombinant strains of Escherichia coli. Biotechnol. Bioprocess. Eng. 10, 378–384.
4. **Calisti, C., Ficca, A.G., Barghini, P., Ruzzi, M.**(2008) Regulation of ferulic catabolic genes in Pseudomonas fluorescens BF13: involvement of a MarR family regulator. Appl. Microbiol. Biotechnol. 80,475-483.
5. **Di Gioia, D., Sciubba, L., Ruzzi, M., Setti, L., Fava, F.**(2009) Production of vanillin from wheat bran hydrolyzates via microbial bioconversion. J. Chem. Technol. Biotechnol. 84, 1441–1448.

CONTACT : Maurizio Ruzzi
ruzzi@unitus.it

Poster a oonçu par : BAOUNE Hafida
baounehafida@hotmail.fr

Présentation orale du poster

Durée moyenne du lecteur :

de 30 sec à 5 minutes …

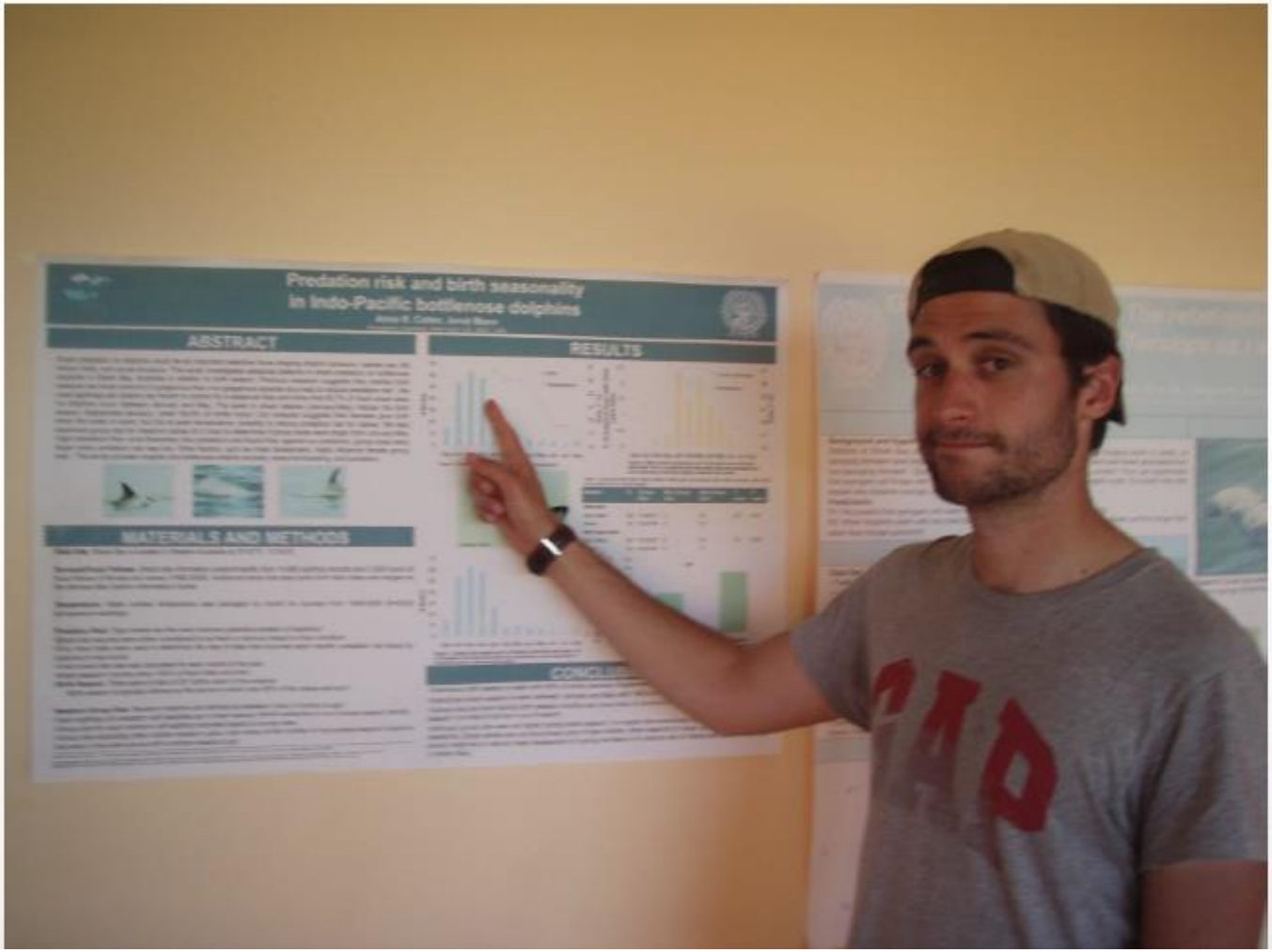

Présentation orale du poster scientifique

- Définir à l'avance le **message** que l'on veut faire passer.
- Utiliser des **phrases courtes** et **claires**.
- Faire des **pauses** après les points importants, en particulier après l'exposition de l'**objectif**.
- **Choisir les mots** avec précaution et surtout de les utiliser de **façon appropriée**.